

CEBAF Program Advisory Committee Seven Update Cover Sheet

This proposal update must be received by close of business on November 23, 1993 at:

CEBAF

User Liaison Office

FAX: (804) 249-5800

12000 Jefferson Avenue

Newport News, VA 23606

Present Conditionally Approved Proposal Title and Number

Measurement of the Flavor Singlet Charge Form Factor
of the Proton, G_E^0 - PR 91-017

Contact Person

Name: DOUGLAS H. BECK

Institution: University of Illinois at Urbana

Address: 23 Stadium Drive

Address: Champaign, IL 61820

City, State ZIP/Country:

Phone: (217) 244-7994

FAX: (217) 333-1215

E-Mail → Internet: beck@uinpla.npl.uiuc.edu

Experimental Hall: c

Total Days Requested for Approval: 164

Minimum and Maximum Beam Energies (GeV): 0.2, 0.3, 0.4, 0.5, 3.0

Minimum and Maximum Beam Currents (μ Amps): 40

CEBAF Use Only

Receipt Date: 11/23/93

PR 93-104

By: g

PAC Update: CEBAF Experiment 91-017, G0

Collaboration

P. Bosted
American University

R. Alarcon, J. Comfort
Arizona State University

B. Filippone, R. McKeown
Caltech

G. Franklin, R. Magahiz, B. Quinn,
R. Schumacher, V. Zeps
Carnegie Mellon University

B. Chen, C. Chu, Q. Chen, M. Fan, H. He,
Z. Ma, Z. Sun, J. Yuan, T. Zhang
China Institute of Atomic Energy

L. Cardman, R. Carlini, D. Mack, M. Musolf
C. Sinclair, W. Vulcan, S. Wood
CEBAF

D. Beck (Spokesman), M. Brussel, R. Eisenstein,
R. Laszewski, A. Nathan, N. Simicevic
University of Illinois

B. Beise
University of Maryland

B. Holstein
University of Massachusetts

J. Napolitano
RPI

Engineering

L. Bartoszek
Bartoszek Engineering

P. Brindza, W. Tuzel
CEBAF

D. Mitchell, R. Wands
Fermilab

A. Langhorn
Star Technologies

November 1993

Contents

1 Overview	1
1.1 Synopsis of PAC update	1
1.2 Synopsis of experiment	3
2 Physics	7
2.1 Introduction	7
2.2 Flavor-dependent nucleon currents	9
2.3 Parity-violating elastic electron scattering	11
2.4 Expected results	14
2.5 Complementarity with Hall A program	17
2.6 Radiative corrections	19
3 Experiment	21
3.1 Introduction	21
3.2 Kinematics and rates	24
3.3 Physics backgrounds	28
3.3.1 Introduction	28
3.3.2 Inelastic protons	29
3.4 Neutrons	33
3.4.1 Pions	36
3.4.2 Inelastic electrons	36
3.5 Room shielding	38
3.6 Compatibility with other Hall C experiments	38
4 Asymmetry Measurement Methodology	40
4.1 Introduction	40

4.2	Data-taking sequence	41
4.3	Statistical uncertainties	41
4.3.1	Beam charge measurement	41
4.3.2	Uncorrelated background noise	43
4.4	Systematic uncertainties and false asymmetries	45
4.4.1	Beam polarization measurement	45
4.4.2	Correlated background noise	45
4.4.3	Corrections for correlated parameter variations	46
4.4.4	Non-linearities	50
4.4.5	Deadtime	51
4.4.6	Pileup	51
4.4.7	Polarized proton scattering in collimators	52
4.4.8	Polarized proton scattering in target	53
4.4.9	Particle counting tests	54
4.5	Analyzing asymmetry data in the presence of background	56
5	Budget	58
5.1	Overall budget	58
5.2	Comparison of Powers Associates and Elin cost estimates	58
6	Schedule	62
7	Beam time request	66
8	Appendix A	68

List of Tables

1	Summary of subsystem responsibilities	6
2	Summary of form factor uncertainties	14
3	Kinematics for forward asymmetry measurement	26
4	Kinematics for backward asymmetry measurement	27
5	Experimental apparatus parameters	27
6	Summary of rates and asymmetries for forward angle measurement	28
7	Summary of rates and asymmetries for backward angle measurements	29
8	Raw inelastic to elastic proton ratio by detector segment	33
9	Beam and spectrometer tolerances	47
10	False asymmetry from collimator scattering of protons	53
11	False asymmetry from target scattering of protons	54
12	G0 budget detail	59
13	G0 Budget Summary	60
14	G0 Budget Contributions	60
15	Spectrometer budget comparison	61
16	Resources for spectrometer fabrication	65
17	Beam time request	66

1 Overview

1.1 Synopsis of PAC update

This update has been prepared for the review of the G0 experiment by the CEBAF Program Advisory Committee.

In this experiment, the parity-violating asymmetry in elastic electron scattering from the proton will be measured at both forward and backward angles and over a range of momentum transfers. These measurements will enable us to determine the contribution of s quarks to the nucleon ground state charge and magnetization densities. A special purpose, superconducting toroidal spectrometer with large azimuthally symmetric angular acceptance is proposed for these measurements.

We request a total of 3940 h of beam time to carry out the separation of the s quark contributions to the nucleon form factors in the region $0.1 \leq Q^2 \leq 0.5 \text{ GeV}^2$. This time is to be utilized as follows:

1. 1100 h for commissioning of experiment
2. 700 h for the forward angle measurement (all momentum transfers simultaneously), and
3. 2100 h for backward angle measurements at $Q^2 = 0.2, 0.3, 0.4$ and 0.5 GeV^2 .

Subsequent to the CEBAF Program Advisory Committee having granted conditional approval to the experiment in January 1993, we have

1. completed a conceptual engineering design for the spectrometer and associated instrumentation,
2. worked to address other concerns of the previous review committees, and
3. had the experiment reviewed by a Technical Advisory Panel (CEBAF, November 18-19, 1993)

Summary responses to the questions previously posed by the PAC and the first 'Barish Committee' review are included in Appendix A.

We have adopted the superconducting design for the spectrometer magnet after concluding that the fabrication costs are only slightly higher than those of a resistive magnet,

and that the operating costs are significantly less than the \$250k per month estimated for the room temperature magnet. The cost of the superconducting magnet is reduced substantially by use of a single, overall cryostat and 'dry', mechanically clamped coils. Full details of the design for the spectrometer and associated instrumentation are available in the G0 Technical Design Report. The design for the experiment has been reviewed extensively by the TAP; a report from that body will be available by the time of the PAC meeting. Important aspects of the conceptual design have also been reviewed by Elin Engieanwendung, contractors for the CEBAF HMS dipole coils; they have also provided a cost estimate. An independent cost estimate has also been made by Powers Associates.

A summary of the important conclusions of our recent studies are as follows (costs are those for complete design, fabrication, assembly and test in North America or Europe):

1. The cost of the spectrometer is estimated to be \$3.061M including 20% EDIA and an overall 25% contingency (constant 1993 \$ assumed throughout).
2. The cost of the detectors, electronics and target is estimated to be \$0.931M.
3. The cost of auxiliary equipment such as beam polarimeter components, beam position monitors, etc. is estimated to be \$0.105M.
4. The total for items 1 - 3 above is \$4.097M (constant 1993 dollars).
5. The total institutional contribution from ongoing grants is \$1.516M (\$0.341M from NSF, \$0.039M from DOE exclusive of CEBAF and \$1.136M from CEBAF operations). **The remaining required support ('new money') amounts to \$2.298M from NSF and \$0.283M from DOE.**
6. Two scenarios for procurement of the spectrometer are being considered:
 - (a) shared fabrication of some elements by UIUC and CIAE at a nominal cost ratio of 60% compared with the 'industrial' price, with UIUC acting as general contractor for industrial procurement of remaining components, and
 - (b) industrial procurement of the complete spectrometer.
7. Assuming significant funding at the beginning of FY95, a two year time scale for fabrication is estimated with beam tests beginning in spring 1997.

This document comprises the following information. This section concludes with an overview of the experiment. A brief summary of the physics is presented in Section 2. The experimental plan is outlined in Sections 3 and 4; the latter section addresses those

special aspects of the experiment related to measurement of parity-violating asymmetries in electron scattering. *The apparatus for the experiment is not described in this document – details may be obtained from the G0 Technical Design Report prepared for the TAP.* This report continues with an outline of cost and schedule aspects of the project. Finally, the beam time request (including an outline of the plan for commissioning) is presented.

1.2 Synopsis of experiment

The structure of the nucleon at low energies is not well understood from the point of view of QCD, i.e. in terms of the quark and gluon degrees of freedom that appear in the QCD Lagrangian. This proposal describes an experiment to measure two ground state proton matrix elements that are sensitive to (point-like) s quarks and hence to the $q\bar{q}$ sea in the proton. The matrix elements of interest are the elastic vector weak neutral current ‘charge’ and ‘magnetic’ form factors, G_E^Z and G_M^Z , respectively, which can be extracted from a set of electron-proton parity-violation measurements. If a relationship between proton and neutron structure is assumed (for example that the proton and neutron differ only by the interchange of u and d quarks, i.e. isospin symmetry), the s quark (as well as the u and d quark) contribution to the form factors of the nucleon can be determined using these weak neutral current form factors and their (measured) electromagnetic counterparts.

Both the charge and magnetic s quark form factors have intrinsic interest as fundamental quantities, as they would constitute the first direct measurements of the quark sea in low energy observables. The goal of the experiment is to determine these contributions to the proton form factors at the few percent level. Observations at high energy suggest that s quarks carry about 1/2 as much momentum as u or d quarks in the sea: it is important to determine both the role of the sea and the relevance of s quarks at low energies where QCD is not understood. Independent of whether the s quarks contribute at the level which is observable in this experiment, it is important to make the measurements. Upper limits at this level provide information as valuable as non-zero determinations. These matrix elements are also relevant to the discussions of the Ellis-Jaffe sum rule and of the πN sigma term; there is evidence in both cases that the s quark contribution is larger than expected. The present measurements will allow the determination of the s quark contributions to proton observables in a much more straightforward manner than in either of the cases noted above.

In this experiment, parity-violating electron scattering asymmetries will be measured in the range $0.1 \leq Q^2 \leq 0.5 \text{ GeV}^2$ at both forward and backward angles. These pairs of measurements will allow us to separate G_E^Z and G_M^Z . The asymmetries range from about -3 to -35×10^{-6} ; we are planning to measure the asymmetries with statistical uncertainties of $\Delta A/A \cong 5\%$ and systematic uncertainties related to helicity correlated

effects of $\Delta A \leq 2.5 \times 10^{-7}$. Initially we will measure concurrently the forward angle asymmetries at five values of momentum transfer in the range $0.1 \leq Q^2 \leq 0.55 \text{ GeV}^2$. Assuming a beam polarization of 49%, the time required to reach this precision for the initial measurement will be about 700 hours. There is good reason to expect that by the time of the experiment higher beam polarizations will be available which would reduce this base time by a factor of two or more. (Using the $G_M^Z(Q^2 = 0.1 \text{ GeV}^2)$ result from the SAMPLE experiment now running at Bates, it would be possible to separate the charge and magnetic form factors in the lowest Q^2 bin after this first measurement.) *Each* subsequent backward angle asymmetry would require from 0.5 - 1 month of running time. We note that the systematic uncertainties quoted for the recent parity measurements at LAMPF, SIN, Mainz and Bates of a few $\times 10^{-8}$ suggest that systematic uncertainties of $\sim 10^{-7}$ should be attainable in this experiment.

To achieve the desired precision in a reasonable amount of time, this experiment must be run at high luminosity with a large-acceptance detector. First, for the forward angle asymmetries, we propose to measure elastically scattered protons ($320 \leq p'_p \leq 797 \text{ MeV}$ with $77.4^\circ \geq \theta'_p \geq 61.2^\circ$, respectively) in order to avoid measurements of electrons at very forward angles (with high luminosities); the electron beam energy will be 3.0 GeV. The solid angle acceptance for the forward angle measurement is 0.9 sr. Second, for the backward angle asymmetries, the spectrometer will be turned around to detect electrons at the complementary angle centered at about 110° with a solid angle acceptance of from 0.9 sr at $Q^2 = 0.2 \text{ GeV}^2$ to 0.5 sr at $Q^2 = 0.5 \text{ GeV}^2$; the beam energies will range from 0.34 to 0.59 GeV. The spectrometer proposed for this experiment provides the unique capability of measuring both the forward and backward angle asymmetries. It consists of a toroidal array of eight superconducting coils with a field integral of approximately 1.6 T·m. The spectrometer is designed to focus particles of the same momentum and scattering angle from the length of the extended target to a single point (zero magnification in the dispersion direction). The bend angle of about 35° at the highest momentum is sufficient to allow complete shielding of the detectors. We expect to be able to count individual particles rather than to integrate the signal in the detectors. Detectors and electronics similar to those planned for the experiment have been bench tested to ensure that counting is feasible (see Section 4.4.9). Particle counting provides the possibility of using time-of-flight to supplement the resolution of the spectrometer. Time-of-flight measurements also require a pulsed beam (31.25 MHz). The detector package for both modes would consist of 14 scintillator elements per segment, each element covering approximately 7% of the full momentum range. In the particle counting mode we also have the option of using pairs of scintillator elements in coincidence.

The spectrometer described above has a number of advantages for this parity-violation experiment. It has very large solid angle and momentum acceptance. The solid angle acceptance is axially symmetric and thus susceptibility to systematic uncertainties is reduced.

The shape of the field is determined by the current conductors, there is no polarized iron in the system, and the magnetic field at the target is zero. Both forward and backward angle asymmetries can be measured with minimal changes in the hardware. The spectrometer is a stand-alone device which would coexist with the Hall C CDR instrumentation thereby providing the stability required for measurements of small asymmetries. It has a relatively simple design and could be fabricated on a reasonably short time scale.

Various types of backgrounds have been investigated for both forward- and backward-angle measurements. In particular, the inelastic proton background was measured at SLAC under essentially the same kinematic conditions. It was found to be approximately consistent with the predictions of Lightbody and O'Connell. These predictions were used in Monte Carlo simulations of the spectrometer which show the inelastic proton contribution to the yield is about 10% or less over the whole kinematic range. The positron background was also measured to be negligibly small. Neutron background has been simulated with the standard codes MCNP and LAHET. In the time bins of interest the neutron contamination relative to the proton elastic signal is expected to be $\lesssim 2\%$. The asymmetry of the combined backgrounds (inelastic protons, neutrons, pions, etc.) is measured simultaneously in time bins which do not contain the elastic protons. In the case of the backward angle measurements where the electrons are detected, the π^- background is kinematically forbidden for the proton target and low incident energies; inelastic electrons are adequately separated from the elastic electrons of interest.

The pattern for data taking will be chosen to reduce random background noise. The standard measurement interval will likely be $1/30$ s (or a minimum in the local noise spectrum); i.e. the beam helicity will be reversed at a frequency of ~ 30 Hz with short intervals between measurements to reverse helicity and read out the spectrometer and the monitors. The helicity pattern $+ - - +$ and its complement will be randomly chosen to reduce further background noise. With this scheme contributions from all harmonics of 30 Hz will be averaged to zero; in addition, long term drifts will be effectively eliminated by averaging the two positive and the two negative helicity measurements in each sequence of four before forming the asymmetry. Data from the spectrometer and beam monitors will be read out at the end of each $1/30$ s measurement interval during the time ($\lesssim 100$ μ s) the beam helicity is being flipped (the experiment will be "gated off" during this time; the beam will continue to run).

The liquid hydrogen target will have a length of about 20 cm. The existing SAMPLE target will be modified for this purpose. With a 40μ A average current the total power deposited by the beam is about 200 W. The SAMPLE target has operated with total dissipated power of about 400 W to date. The beam will be rastered over a target area of about 0.2 cm^2 – comparable to that in the SAMPLE experiment.

Table 1: Summary of responsible institution and individual for instrumentation subsystems.

Source construction	CEBAF, L. Cardman
Source, accelerator instrumentation	CEBAF, C. Sinclair
Beamline instrumentation	CEBAF, R. Carlini
Target	Maryland/Caltech, B. Beise
Spectrometer	UIUC, R. Laszewski; CIAE, M. Fan
Detectors	RPI, J. Napolitano
Electronics, DAQ	CMU, B. Quinn
DAQ	CEBAF, S. Wood
Simulation software	ASU, R. Alarcon

Precise monitoring and control of the beam will be required for this experiment. For each measurement interval the beam characteristics – position, angle, energy and charge must be measured. Based on the present design of the experiment, position measurements with precision on the order of $25 \mu\text{m}$ will be required for each measurement interval (the most stringent requirements are for the position measurements used to determine the beam energy centroid). During the experiment continuous monitoring of false asymmetries due to changing beam characteristics will require substantial interaction with various accelerator controls, including, for example, some control of steering in the beam switchyard.

The collaboration brings much experience in both electron scattering and parity-violation experiments, in the instrumentation necessary for the experiment, and in knowledge of the CEBAF accelerator. Arizona State is undertaking the GEANT and TOSCA simulations. The Caltech and Maryland groups will be responsible for the target. The Carnegie Mellon collaborators will provide the data acquisition electronics. CEBAF takes responsibility for accelerator and beamline instrumentation as well as general experimental support. In addition CEBAF will make a substantial contribution to the overall cost of the new instrumentation. The spectrometer will be designed and constructed by the University of Illinois and the China Institute of Atomic Energy. Illinois has also provided the polarized electron source for the accelerator. The detectors will be built at RPI. Theoretical support will be provided by Musolf and Holstein, with particular emphasis on the radiative corrections. A summary of the responsibilities for the experimental subsystems is presented in Table 1.

2 Physics

2.1 Introduction

There is strong experimental evidence that the quarks and gluons of the QCD Lagrangian are observed in deep-inelastic scattering and high energy e^+e^- annihilation among other processes. This is the regime in which the interactions of quarks are weak; it is “QED-like” in the sense that perturbation theory is a suitable tool. However, at low energies, QCD exhibits at least two properties which make it very different from QED, those of confinement and spontaneous chiral symmetry breaking. Here perturbation theory is not suitable and much effort has gone into discretization (lattice) and other techniques to try to understand QCD in the strong coupling regime. The purpose of this experiment is to make a low energy measurement of a quantity precisely defined in the context of QCD.

At low energies (corresponding to distance scales ~ 1 fm) little is known about the detailed structure of hadrons within the framework of QCD. As effective degrees of freedom, constituent quarks have proven to be very successful in categorizing and understanding the spectra of baryons and mesons. Neither the general properties of constituent quarks nor their relationship to the quarks of QCD are well understood. For example, how large is a constituent quark? What are its charge and magnetic moment densities? Does it have any “excited” states? [We90] How does it respond to its environment (or, for example, are the constituent quarks in the nucleon and the pion the same)? One of the other successfully demonstrated consequences of QCD at low energies is the near chiral limit in which pions (at least) play the role of Goldstone bosons. [Do89] This “chiral perturbation theory” leads to the recovery of the current algebra phenomenology of strong interactions. The relationship of this language to that of constituent quarks is not clear, although some connection can be made through the “chiral quark” effective Lagrangian of Manohar and Georgi. [Ma84a]

In this experiment an approach will be made from a different direction to try to gain some insight into the consequences of QCD at low energies. The $q\bar{q}$ sea, whose importance at these energies is relatively unknown, is subsumed in effective degrees of freedom in all of the pictures described above. Because this measurement is sensitive to s quark contributions, and because s quarks are restricted to the sea in the nucleon, it can provide direct information on the importance of the $\bar{q}q$ sea at low energies. We note that even upper limits on the s quark contribution of a few percent (in this experiment determined directly), should that be the result, are as important as, for example, the indications of s quark contributions of tens of percent from other experiments discussed below.

There is some experimental evidence that suggests the s quark contribution to various

proton matrix elements is significant (notably the Ellis-Jaffe sum rule measurements [Ad93, An93, As89] though the evidence here is mixed and the πN sigma term [Do89]). These measurements determine axial-vector and scalar s quark current matrix elements in the proton; the related quantity in this experiment is the vector s quark current matrix element. That s quarks are present in the nucleon is not an issue – deep inelastic measurements [Ab82] show that they carry about 3% of the nucleon’s momentum or about half the average momentum carried by u and d sea quarks. The plausibility of significant s quark contributions to low momentum transfer matrix elements is reinforced by the fact that these same deep inelastic measurements show that the momentum distribution $s(x)$ diverges as $x \rightarrow 0$ (corresponding roughly to the large size components of the nucleon wave function).

The proposed experiment will measure the parity-violating asymmetries in elastic electron-proton scattering at momentum transfers between $0.1 \leq Q^2 \leq 0.5 \text{ GeV}^2$. These asymmetries depend on both the electromagnetic proton form factors, G_E and G_M , and the analogous neutral weak current form factors, G_E^Z and G_M^Z . From the neutral weak current form factors and the measured electromagnetic form factors of the proton, one can extract the so-called flavor singlet form factors, $G_{E,M}^0$ which characterize the difference between the corresponding electromagnetic and weak form factors. These form factors are determined by proton form factors *only* (including those from this measurement) and are therefore independent of the less well known neutron form factors and of a model linking the proton and neutron.

Alternately, one can combine the electromagnetic form factors of the proton and neutron with the weak neutral current form factors of the proton and determine the s quark contributions to the form factors (as indicated below). Asymmetries will be measured at both forward and backward angles using the same spectrometer to enable us to separate the charge and magnetic form factors in each case. It should be noted that the only assumptions required to extract the s quark components of the form factors are that the quarks are point-like (and that we know their charges), that c and heavier quarks do not contribute significantly and that there exists a model relating proton and neutron structure.

Little is known about the nucleon s quark (or, equivalently, the flavor singlet) form factors. Only the normalization of the s quark contribution to the charge form factor is known – since the proton has no net strangeness, $G_E^{s,p}(Q^2 = 0) = 0$. Neither the normalization of $G_M^{s,p}$ nor the Q^2 dependences of either form factor are constrained by experiment. There are preliminary results of an analysis [Ga93] of the Brookhaven E734 [Ab87] $p(\nu, \nu)$ experiment, which indicate that the G_E^s and G_M^s are small averaged over the momentum transfer range $0.5 \leq Q^2 \leq 1.0$ (see Section 2.4).

In principle, the asymmetry is sensitive to deviations from the Standard Model as well as to hadronic structure. However, the effect from possible new physics beyond the

Standard Model is expected to be about an order of magnitude smaller than what might be expected from s quarks at these momentum transfers (although both estimates are obviously crude). If the ‘expected’ results for G_E^0 and G_M^0 are obtained with a high degree of precision, it might then be possible to design a set of experiments optimized to determine all the hadronic structure physics necessary to search for departures from the Standard Model.

2.2 Flavor-dependent nucleon currents

The electroweak probe provides a precise means of studying the currents of point-like quarks inside the nucleon. Because they are assumed to be Dirac particles in QCD, their (vector) currents are written simply as

$$\mathcal{J}_\mu^{ew} = \mathcal{Q} \bar{q} \gamma_\mu q$$

where \mathcal{Q} is the charge appropriate to γ (ordinary electromagnetic charge) or Z^0 (neutral weak “charge”, see below) coupling. The total electroweak current of the nucleon can then be written as a sum of the contributions from each of the quark flavors. [Ca78, Ka88, Mc89, Be89, Na91, Mu93b] For example, the electromagnetic form factors can be divided up in this way

$$G_{E,M}^{p,\gamma} = \sum_j \mathcal{Q}_j G_E^{j,p}$$

where j runs over all quark flavors and \mathcal{Q}_j is the electric charge. (We note that this is an exact statement.) In what follows the contributions of the quarks and antiquarks of a given flavor are combined. For example, $G_E^{u,p}$ will represent the net contribution of u and \bar{u} quarks to the charge form factor. The expression for the electromagnetic form factors is then

$$G_{E,M}^{p,\gamma} = \frac{2}{3} G_{E,M}^{u,p} - \frac{1}{3} G_{E,M}^{d,p} + \dots$$

The utility of measuring the corresponding weak neutral current of the nucleon (in this case via parity-violating electron scattering, see Section 2.3) is that it can also be written in terms of the $G_{E,M}^{j,p}$

$$G_{E,M}^{p,Z} = \sum_j \left(\frac{1}{2} T_j^3 - \mathcal{Q}_j \sin^2 \theta_W \right) G_{E,M}^{j,p}$$

where $(1/2T_j^3 - Q_j \sin^2 \theta_W)$ is the weak “charge”. This in turn suggests that the contributions of the quark flavors may be separated experimentally.

In order to determine $G_E^{s,p}$ or $G_M^{s,p}$, the s quark vector current matrix elements of the proton (“ s quark form factors”), *three* measurements are required (in addition to the assumption that c and heavier quarks do not contribute significantly). In addition to the form factors $G_E^{p,\gamma}$ and $G_E^{p,Z}$ it is possible to make use of $G_E^{n,\gamma}$ if a model of the relation between proton and neutron structure is assumed. The simplest relationship is that interchanging u and d quarks will transform a neutron into a proton and vice versa (isospin symmetry), i.e., in this language

$$\begin{aligned} G_{E,M}^{u,p} &= G_{E,M}^{d,n} \\ G_{E,M}^{d,p} &= G_{E,M}^{u,n} \\ G_{E,M}^{s,p} &= G_{E,M}^{s,n} \end{aligned}$$

The s quark form factors are then

$$G_{E,M}^s = (1 - 4 \sin^2 \theta_W) G_{E,M}^{p,\gamma} - G_{E,M}^n - 4G_{E,M}^{p,Z}$$

with similar expressions for the u and d quark form factors. We note that this experiment will allow the three pairs of form factors $G_{E,M}^{\gamma,p}$, $G_{E,M}^{\gamma,n}$ and $G_{E,M}^{Z,p}$ to be written as the set $G_{E,M}^u$, $G_{E,M}^d$ and $G_{E,M}^s$. The u and d form factors, combinations of valence and sea contributions, also contain interesting information. The non-zero neutron charge radius, for example, suggests rather different u and d form factors. [Be92]

It is possible that s quarks could show up in either G_E or in G_M if they are significant. In order to contribute to the charge form factor there must be a ‘polarization’ of the s and \bar{s} distributions, i.e. they must have different spatial distributions. The presence of s and \bar{s} with different angular momenta – opposite m_l , for example – would result in a contribution to G_M . A variety of combinations is therefore plausible in which s quarks would contribute more to one form factor than the other. It should be noted that at present no microscopic model is capable of realistically linking the contributions to the charge and magnetic form factors.

The experiment may also be discussed in a model-independent framework. Since the electromagnetic and weak neutral currents of the nucleon are related, it is natural to ask what new information is contained in the $G_{E,M}^{p,Z}$. For this purpose it turns out to be useful to rewrite the individual flavor contributions in terms of an SU(3) flavor basis. The electromagnetic form factors are then

$$G_{E,M}^{p,\gamma} = G_{E,M}^{3,p} + \frac{1}{\sqrt{3}} G_{E,M}^{8,p}$$

where

$$G_{E,M}^{3,p} = \frac{1}{2} (G_{E,M}^{u,p} - G_{E,M}^{d,p})$$

are the ordinary isovector form factors, and

$$G_{E,M}^{8,p} = \frac{1}{2\sqrt{3}} (G_{E,M}^{u,p} + G_{E,M}^{d,p} - 2G_{E,M}^{s,p})$$

are the octet contributions. In this basis the neutral weak form factors are

$$\begin{aligned} G_{E,M}^{p,Z} &= \left(\frac{1}{2} - \sin^2 \theta_w \right) G_{E,M}^{3,p} + \left(\frac{1}{2\sqrt{3}} - \frac{1}{\sqrt{3}} \sin^2 \theta_w \right) G_{E,M}^{8,p} - \frac{1}{4} G_{E,M}^{0,p} \\ &= \left(\frac{1}{2} - \sin^2 \theta_w \right) G_{E,M}^{p,\gamma} - \frac{1}{4} G_{E,M}^{0,p} \end{aligned}$$

where

$$G_{E,M}^{0,p} = \frac{1}{3} (G_{E,M}^{u,p} + G_{E,M}^{d,p} + G_{E,M}^{s,p})$$

are the flavor singlet proton form factors. Therefore, the new information in the measurements is the flavor singlet current. It, along with the octet current, is sensitive to s -quark contributions.

At this stage there are no reliable microscopic models of the nucleon which could predict any such distributions. The phenomenological model of Jaffe [Ja89] in which the dispersion theory based approach of Höhler *et al.* [Ho76] is extended to include a strange vector meson, the $\phi(1020)$, is apparently in disagreement with the recent analysis of the E734 neutrino scattering data (see Section refsubsec:precision. Attempts have also been made to consider the contributions from the point of view of kaon admixtures in the nucleon wave function, both in the SU(3) Skyrme model [Pa91] and in $\Lambda\kappa$ admixture models. [Mu93a, Co93] These models give generally small results. A recent cloudy bag model calculation [Ho93] predicts a rather large positive $G_M^s(Q^2 = 0)$ of 0.4 n.m. whereas most of the other models predict comparable negative values.

2.3 Parity-violating elastic electron scattering

Electron scattering by current distributions is described by the coherent sum of γ and Z^0 amplitudes

$$\mathcal{M} = \mathcal{M}^\gamma + \mathcal{M}^Z$$

although we tend to ignore \mathcal{M}^Z since it is very small, roughly 10^{-5} as large as \mathcal{M}^γ . However, \mathcal{M}^Z , unlike \mathcal{M}^γ , has both vector and axial-vector pieces. Therefore, the cross term in the cross section violates parity.

The cross term can be determined experimentally by comparing two parity-sensitive cross sections whose parity-conserving parts are identical. In this case the two cross sections are those of longitudinally polarized electrons with positive and negative helicities. Because the parity-violating terms in the cross sections are proportional to the electron helicity, the asymmetry is directly related to the cross term, i.e.

$$A = \frac{\sigma_+ - \sigma_-}{\sigma_+ + \sigma_-} \propto \mathcal{M}^\gamma \mathcal{M}^Z / |\mathcal{M}^\gamma|^2.$$

In terms of the form factors defined earlier, the asymmetry for elastic $\vec{e}p$ scattering is [Ca78, Mc89, Be89, Na91, Mu93a]

$$A = -\frac{G_F Q^2}{\pi \alpha \sqrt{2}} \{A_E + A_M + A_A\} / A_D$$

where

$$\begin{aligned} A_E &= \varepsilon G_E^\gamma G_E^Z, \\ A_M &= \tau G_M^\gamma G_M^Z, \\ A_A &= -\frac{1}{2}(1 - 4\sin^2\theta_W)\sqrt{\tau(1+\tau)(1-\varepsilon^2)}G_M^\gamma G_A^Z, \\ A_D &= \varepsilon(G_E^\gamma)^2 + \tau(G_M^\gamma)^2, \end{aligned}$$

and

$$\varepsilon = [1 + 2(1 + \tau)\tan^2\theta/2]^{-1}$$

Note that ε can be varied between zero and unity for a fixed Q^2 by varying the beam energy and electron scattering angle. The ‘‘axial-vector’’ term proportional to G_A^Z arises from the axial-vector current in the proton which may couple directly to the Z^0 . Note that it is suppressed relative to the vector ‘‘electric’’ and ‘‘magnetic’’ terms because of the factor $(1 - 4\sin^2\theta_W) \approx 0.08$.

Knowing G_A^Z [Ba81, Mi82, Ki83], it is possible separate G_E^Z and G_M^Z by making asymmetry measurements at the same momentum transfer but different values of ε . Figure 1 shows the contributions of each of the three terms to the asymmetry for the lowest and highest momentum transfers proposed. This plot is analogous to the Rosenbluth plot for ordinary electron scattering. Note that the magnetic term, A_M , dominates the asymmetry over the range of the experiment. In particular, it is therefore not possible to extract information about G_E^Z with forward angle measurements alone. For this experiment, $\varepsilon = 0.95 - 0.99$ for the forward angle measurements and $\varepsilon \cong 0.2$ at back angles.

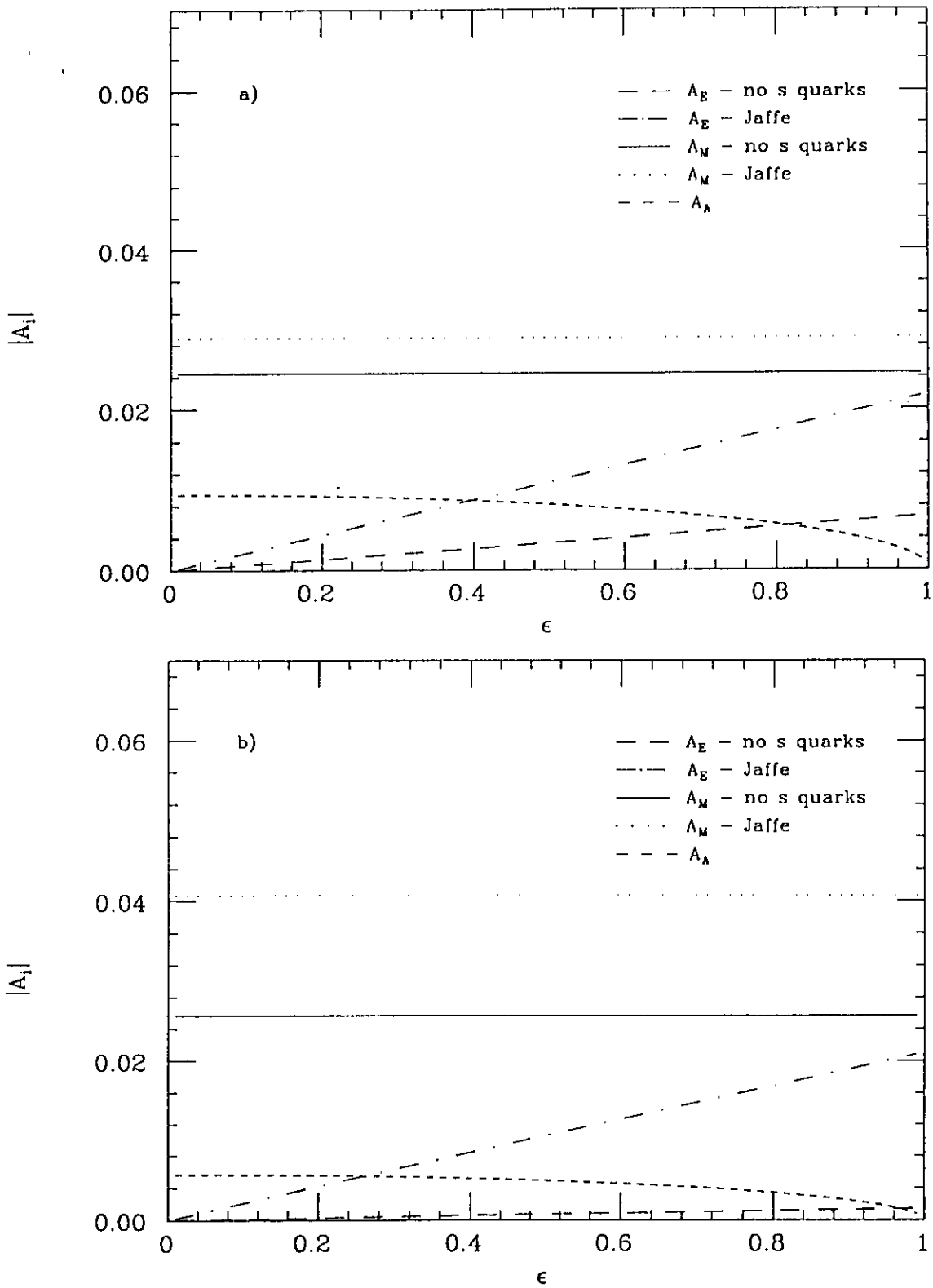


Figure 1: "Rosenbluth" plot of the parity-violating asymmetry showing the contributions of the three terms for a) $Q^2 = 0.1 \text{ GeV}^2$, and b) $Q^2 = 0.5 \text{ GeV}^2$. The terms A_E and A_M are shown for both no s quarks and the Jaffe [Ja89] model. All asymmetry contributions are positive except $A_E(Q^2 = 0.5)$ for no s quarks.

Table 2: Summary of proton and neutron form factor uncertainties used to obtain the results for G_E^s and G_M^s shown in Figures 2 and 3. Note the improved precision listed for G_E^n and G_M^n – such measurements are planned for CEBAF. Note also that the uncertainty listed for G_A^Z corresponds to that of its radiative correction as discussed in Section 2.6.

Quantity	Uncertainty (%)
$\Delta G_E^{p,\gamma} / G_E^{p,\gamma}$	2
$\Delta G_M^{p,\gamma} / G_M^{p,\gamma}$	2
$\Delta G_E^{n,\gamma} / G_E^{n,\gamma}$	20
$\Delta G_M^{n,\gamma} / G_M^{n,\gamma}$	3
$\Delta G_A^{p,Z} / G_A^{p,Z}$	10

2.4 Expected results

The expected results from the experiment are summarized here. The details of the experimental parameters such as kinematics, luminosity, acceptances, rates and asymmetries are presented in Section 3.2. In Figures 2 and 3 the expected results are shown for the s quark form factors G_E^s and G_M^s assuming pn isospin symmetry and the experimental parameters as listed in Tables 3.1–3.5. (The backward angle asymmetry required at $Q^2 = 0.125 \text{ GeV}^2$ is taken from the expected result of the SAMPLE experiment.) In addition, the uncertainties in the proton and neutron form factors needed to extract G_E^s and G_M^s are listed in Table 2. The uncertainties shown do not include systematic uncertainties (which are expected to be small relative to the statistical uncertainties for $Q^2 \geq 0.2 \text{ GeV}^2$) nor do they include uncertainties in the radiative corrections for the weak *vector* form factors (the large uncertainty in the axial-vector form factor *is* included). It should be noted that whereas the uncertainty in G_E^s is dominated by the statistical uncertainty in this experiment, there are roughly equal contributions to the G_M^s uncertainty from the combination of statistics and uncertainties in $G_M^{n,\gamma}$ and $G_A^{p,Z}$. We note that with a possible improvement of a factor of 2.5 in the figure of merit from the polarized source, the uncertainties for G_E^s would then have equal contributions from statistics and the uncertainty in G_E^n .

Also shown in these Figures are the preliminary results from the reanalysis of the Brookhaven E734 experiment. [Ga93] These determinations of the form factor result from fits to the ν and $\bar{\nu}$ proton elastic scattering data (note that 79% of the protons in the target were bound in ^{12}C and ^{27}Al) to extract, effectively, the three form factors G_E^s , G_M^s and G_A^s along with the axial vector dipole mass parameter M_A and two overall scale

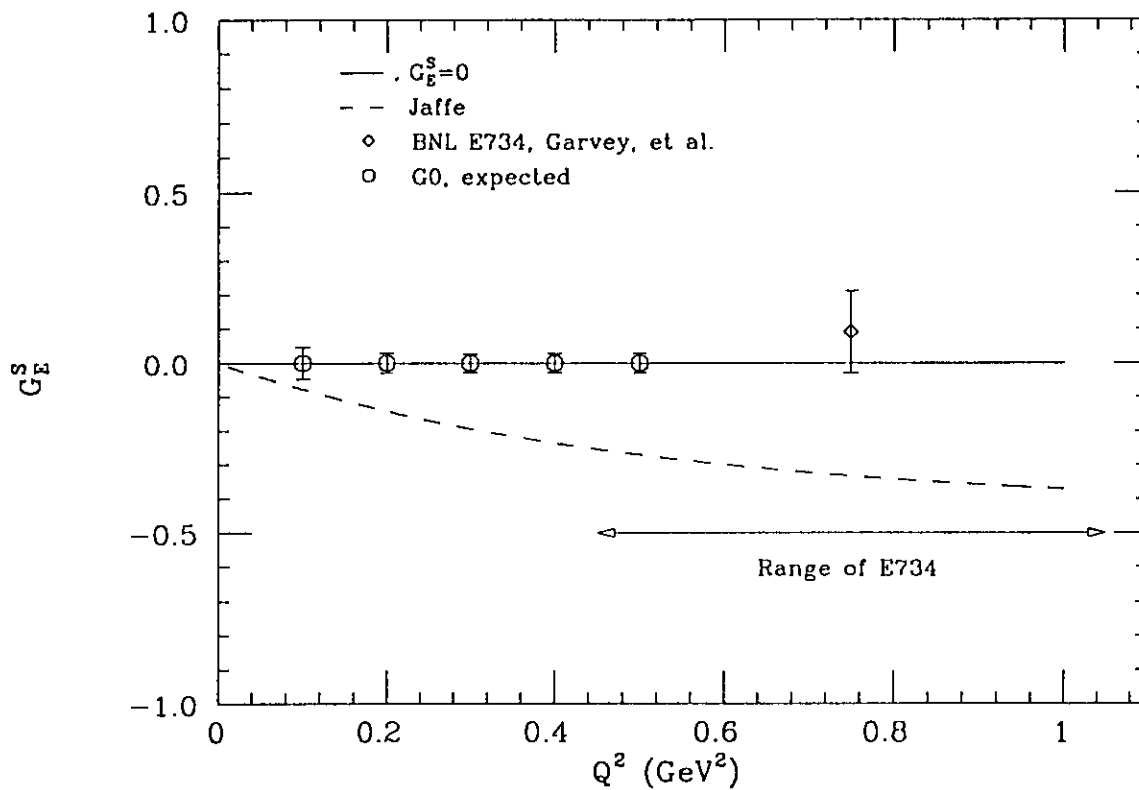


Figure 2: Expected result for G_E^s assuming pn isospin symmetry, the experimental parameters of Section 3.2 and the uncertainties in the proton and neutron form factors listed in Table 2 for $G_E^s(Q^2) \equiv 0$ and the model of Jaffe [Ja89].

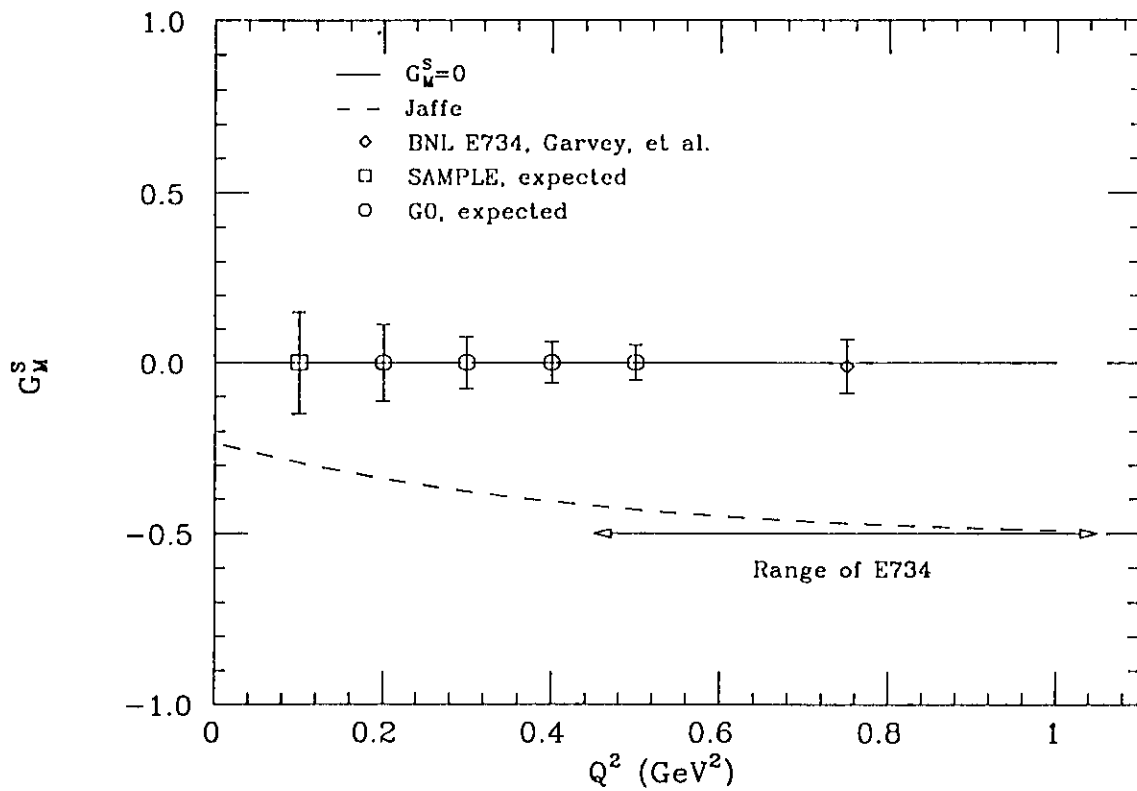


Figure 3: Expected result for G_M^s assuming pn isospin symmetry, the experimental parameters of Section 3.2 and the uncertainties in the proton and neutron form factors listed in Table 2 for $G_M^s(Q^2) \equiv 0$.

parameters. Because there is a term in the cross section that is proportional to $G_A G_M^Z$, and this term changes signs for $\bar{\nu}$ relative to ν , G_M^Z and hence G_M^* , determined by the cross section difference, is the most precise result of the analysis. The fits assume a simple dipole parameterization of the s quark form factors with the same mass as the overall dipole form factors (though some related forms were tested with similar results). The uncertainties shown for these data are from statistics and both overall normalization as well as Q^2 dependent systematic experimental uncertainties; no uncertainties are included for model dependence.

Back angle asymmetries may also be measured for $0.5 < Q^2 \lesssim 3 \text{ GeV}^2$ by adjusting the collimators to limit the angular acceptance and retain the separation of the elastic and inelastic electrons. Useable effective solid angles vary from about 0.5 sr for $Q^2 = 0.5 \text{ GeV}^2$ to 0.28 sr at $Q^2 = 3 \text{ GeV}^2$. The uncertainties anticipated for such measurements with one month of beam time per measurement are shown in Figure 4. We note that because the asymmetries are increasing with Q^2 , the systematic uncertainties are less significant than in the lower Q^2 measurements above. Higher Q^2 forward asymmetry measurements using *lower* incident energies may also be possible with comparable statistical precision and reduced Q^2 resolution (see the Technical Design Report, Section 8.3.11). Lower Q^2 measurements will also be possible, limited by the minimum detectable proton energy. With kinetic energies of 30 MeV, protons will lose about 1/2 of their energy exiting the spectrometer and stop in the detector scintillators – this lower limit corresponds to $Q^2 = 0.056 \text{ GeV}^2$.

2.5 Complementarity with Hall A program

The plans of the Hall A collaboration [Fi91] to measure forward asymmetries for the proton at momentum transfers between about 0.3 and 1.3 GeV^2 complement the present measurements well. There will be some overlap in the forward asymmetries and their measurements, combined with the back angle asymmetries from the present experiment for momentum transfers above 0.5 GeV^2 will enable us to extend the separation of G_E^Z and G_M^Z significantly. The projected uncertainties of about 5% in the asymmetry are comparable to those from the higher Q^2 G0 measurements.

There are also plans for forward ^2H and ^4He measurements [Fi91, Be91] in Hall A. A comparison of nucleon form factors determined from all experiments will be useful to, among other things, set limits on changes in these nucleon properties in nuclei.

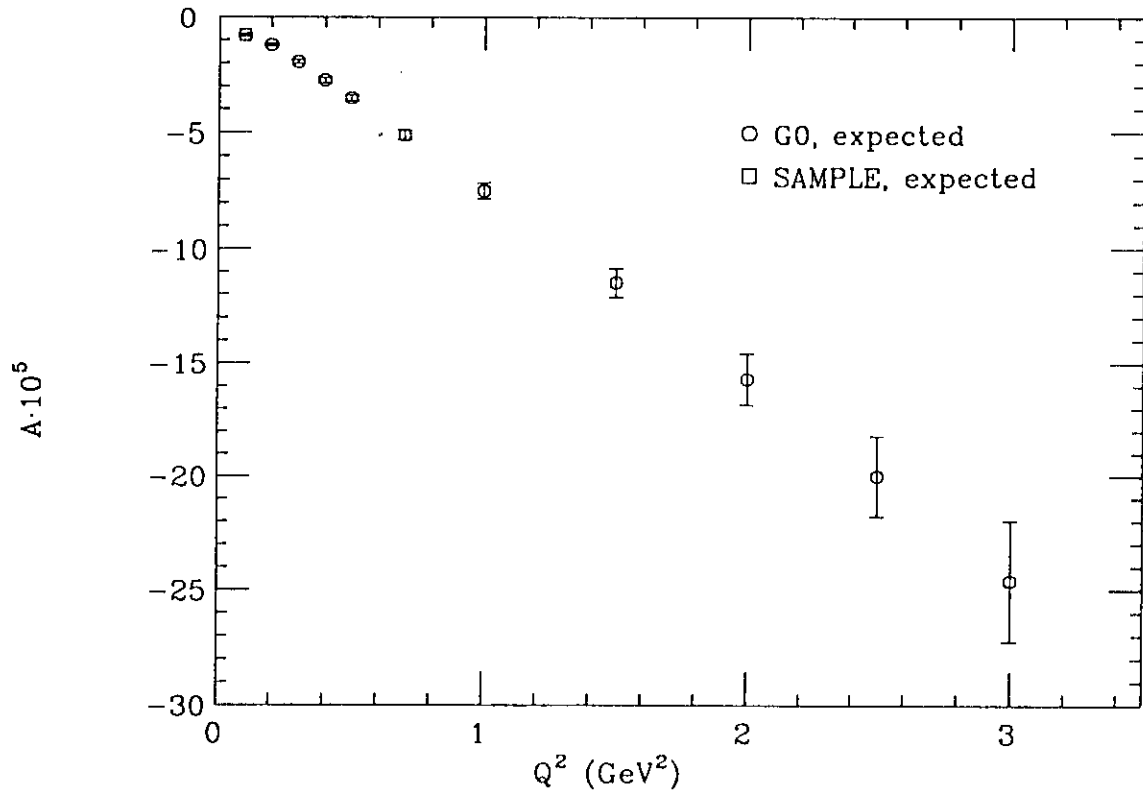


Figure 4: Expected results for possible high Q^2 back angle asymmetry measurements. The experimental parameters of Section 3 are assumed; the running time for each point is 700 h.

2.6 Radiative corrections

A proper interpretation of precision measurements of the hadronic neutral current requires that one take into consideration corrections to “tree-level” formulae introduced by higher-order electroweak processes. While the scale of these corrections is generically of $O(G_\mu\alpha/4\pi)$ at one-loop order, their importance relative to the tree-level amplitudes can be enhanced by the presence of large logarithms in one-loop amplitudes and by accidental numerical suppression of tree-level terms. [Mu90] In addition to carrying a dependence on the undetermined Higgs and t quark masses, electroweak corrections can also depend on theoretically uncertain hadronic physics. While (M_H, m_t) uncertainties introduce no fundamental limitation on the interpretation of precise electron scattering parity-violation experiments, hadronic uncertainties can represent a more serious issue in certain kinematic situations. One must be clear, then about where the latter uncertainties arise and to what extent they limit the information which might be extracted from precision measurements. The ep elastic asymmetry presented in Section 2.3 depends on three terms each of which has an associated electroweak radiative correction. The corrections for G_E^Z and G_M^Z may be calculated with good precision; the correction for G_E^Z is several times larger than that for G_M^Z . For example, the calculation of the correction factor for G_E^Z , defined by

$$G_E^{Z, meas} = G_E^{Z, tree}(1 + R_E)$$

gives $R_E = -0.33 \pm 0.01$; [Mu90] the scale of the uncertainty is estimated from the work of Marciano and Sirlin. [Ma84b]

The potential source of difficulty for the present measurement is the relatively much less certain radiative correction for G_A^Z . The correction is estimated to be $R_A = -0.24 \pm 0.22$, [Mu90] where the uncertainty cited is only an informed guess.

An additional measurement can be made with the same apparatus, however, to improve our knowledge of this correction. The parity-violating asymmetry in quasielastic scattering from the deuteron at backward angles emphasizes the A_A term in the asymmetry [Ha92]. As discussed in Section 3, such a measurement will allow us to at least confirm the uncertainty at the level somewhat better than that cited above. Quasielastic scattering from deuterium at backward angles is advantageous in that the s quark (isoscalar) effects enter multiplied by essentially $\mu^p + \mu^n = 0.88$ and the axial form factor (including its radiative correction) enters multiplied by essentially $\mu^p - \mu^n = 4.7$. Therefore, in such a measurement the unknown s quark effects are suppressed relative to the unknown axial form factor radiative corrections. The roughly 3% uncertainty in the neutron magnetic form factor G_M^n measurements to be done at NIKHEF, Mainz and CEBAF restricts interpretation of this deuteron quasielastic asymmetry at the level of $\sim \pm 0.1$ for the radiative correction.

The ordinary radiative effects which enter into normal electron scattering experiments do not enter the asymmetry to first order. They do, however, affect the rates in that each cross section will be reduced by, in our case, about 15%. Therefore, the nominal running times for the experiment have been increased by the appropriate factor.

3 Experiment

3.1 Introduction

In this experiment the parity-violating asymmetry in elastic electron-proton scattering will be measured at forward and backward angles in the Q^2 range of 0.1 to 0.5 GeV². Because the asymmetries in such experiments are small, a large counting rate is required. In the present case the measured asymmetry will be a few $\times 10^{-6}$ and in order to achieve a statistical precision of 5% of this asymmetry approximately 10^{13} counts will be needed. The large counting rate is generally obtained by using a combination of high luminosities and detectors with large acceptances. In the present experiment a 20 cm long LH₂ target will be used with a 40 μ A beam current ($\mathcal{L} = 2.1 \times 10^{38}$ cm⁻² s⁻¹) and a detector with a solid angle acceptance of 0.9 sr for the forward angle measurements and 0.5 - 0.9 sr for those at back angles.

In order to perform the most precise separation of G_E^Z and G_M^Z it is advantageous to

1. measure forward angle asymmetries for values of ϵ as near to 1 as possible (it can be seen from Figure 2.1 that the axial contribution drops only near $\epsilon = 1$) and,
2. measure backward angle asymmetries with small ϵ to increase the lever arm as much as possible.

The first requirement implies very forward electron scattering angles at these momentum transfers, and this condition is in turn difficult to handle given the requirement for high luminosities and large solid angle acceptances. The condition of large ϵ can also be met by detecting the recoil protons at relatively large angles which is the choice for this experiment. The second requirement can be met by detecting electrons at the complementary angle to that of the recoil protons (operationally by turning the spectrometer 'end-for-end' relative to the beam direction) because ϵ does not vary rapidly with angle in the backward direction ($\epsilon \cong 0.2$ for the kinematics of this experiment).

Further, the recoil protons and elastic electrons for the conditions set out above have roughly the same momentum for the Q^2 range of interest. The maximum momentum of the spectrometer is chosen to match the maximum proton momentum ~ 800 MeV; this range of momentum also allows the spectrometer to be used to measure backward asymmetries as high as $Q^2 \cong 3$ GeV² (see Section 2.4). For these moderate momenta, a relatively simple spectrometer of very large acceptance can be designed (see Technical Design Report). Another important characteristic of this spectrometer is the choice of zero

magnification optics, $(x|x) = 0$,¹ rather than the point-to-point optics common in dipole spectrometers. This allows us to use a long target while preserving a large solid angle acceptance.

In particular, this spectrometer has been designed to minimize the overall experimental running time by taking advantage of rapid variation of Q^2 with proton angle in the forward measurement combined with a solid angle acceptance which is nearly as large for each of the back angle measurements. As can be seen in Figure 5, the momentum transfer in the forward measurement varies from about 0.1 to about 0.55 over the range of proton angles from 80° to 60° ; in the backward measurements, however, the momentum transfer varies slowly (as it does for all angles backward of $\sim 60^\circ$). The spectrometer is designed to measure the entire range of momentum transfers in a single forward measurement. Such a strategy is impossible for the back angle. Therefore, the objective for the back angle measurements is to maximize the total angular acceptance without adversely effecting the range of the forward measurement.

To illustrate the present balance, it is useful to consider an example in which the same experimental results are obtained and the total running time (presently one month forward plus three months backward) is reduced by 25% by increasing the back angle acceptance. Increasing the back angle acceptance significantly would lead to a reduction in the Q^2 range of the forward measurement (as discussed below) such that (at least) two forward measurements would be required. For this example the back angle acceptances would have to increase by a factor of three to obtain the 25% beam time reduction! An increase from 0.9 to 2.7 sr (corresponding to a scattering angle acceptance of about 55°) at the lowest momentum transfer in the backward direction seems unlikely. We present below a simple argument which suggests that significant increases in the back angle acceptance make the forward angle measurements (and the whole experiment) much more time consuming.

The primary requirement for the back angle measurements is resolution of the elastic and inelastic electrons. Ideally, one would like to place all elastic electrons at the same point on the focal plane and all inelastic electrons, whose energy roughly tracks that of the elastic electrons, in some separate region. Schematically this could be accomplished by using the matrix elements $(x|p)$ and $(x|\theta)$ to account for the kinematic variation of final elastic electron energy as a function of scattering angle, i.e. one would like to set the variation of x with respect to the elastic energy equal to zero. To lowest order the position at the focal plane is

$$x = x_0 + (x|p)(p(\theta) - p_0) + (x|\theta)(\theta - \theta_0).$$

¹To be precise the focal plane is defined by the minimum of $(x|x)$ for a given point in the plane normal to the trajectories.

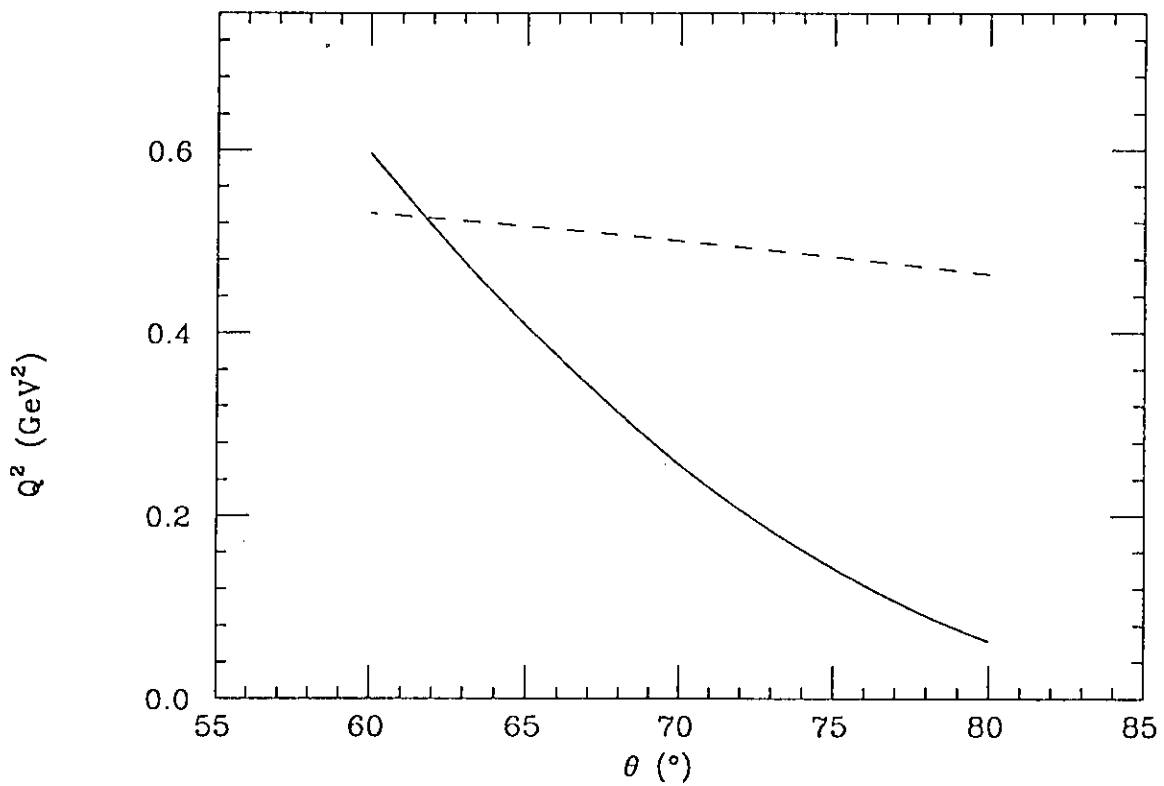


Figure 5: Forward (solid) kinematics for proton detection. Back angle (dashed) kinematics, for example, at $Q^2 = 0.5 \text{ GeV}^2$ (θ for back angle is complement of actual scattering angle).

The desired condition can then be expressed (to the same order) as

$$\frac{dx}{d\theta} = (x|p)\frac{dp}{d\theta} + (x|\theta) = 0.$$

Now, for a toroidal spectrometer similar to the one proposed here the matrix elements are on the order of $+0.5$ cm/MeV (~ 2.5 cm/%) and -0.5 cm/mr, respectively, but the derivative is small: $dp/d\theta \sim -0.1$ MeV/mr. Therefore, it is very difficult, even in first order, to group all the elastic electrons from a large angular bite in a small region of the focal surface without reducing $(x|\theta)$ by an order of magnitude (while changing its sign and keeping $(x|x) \cong 0$) or increasing $(x|p)$ by the same amount (or some combination of the two). Increased dispersion $(x|p)$ would reduce the Q^2 range in the forward measurement for a fixed detector size. Since significant changes in this quantity are called for, two or more forward measurements would be required to cover the Q^2 range of interest. We note finally that increasing the dispersion and enlarging the detectors significantly is ultimately limited in an azimuthally symmetric device because of the fixed distance from the beam line to the floor.

There are also several advantages accruing from the spectrometer and the design for the experiment that are particularly useful for measurements of small asymmetries. It is azimuthally symmetric thus the sensitivity to systematic errors associated with beam motion is minimized. Forward and backward angle measurements can be made with the same device. The spectrometer has no magnetized iron, therefore, false asymmetries due to secondary scattering will not be a problem. There is zero magnetic field at the target position. It is a standalone device which will provide the stability of setup important to such measurements. Finally, this spectrometer is small enough to be positioned upstream of the pivot in Hall C so that interference with other experiments will be minimal.

In addition to the need for large rate, the experiment must be designed to reduce systematic errors to an acceptable level – the goal also being $\Delta A \leq 2.5 \times 10^{-7}$ from helicity correlated effects, or about 5% or less of the measured asymmetry. This requires precise monitoring of beam characteristics such as position, angle, shape, energy and intensity as well as spectrometer acceptance, counting rates and backgrounds. The effects of each item on this list are described below in Sections 3.3 4.3 and 4.4. The beam monitors are also described in the Technical Design Report Section 6.4.

3.2 Kinematics and rates

The basic layout of the forward angle experiment is shown in Figure 6. Polarized electrons scatter from the target cell; recoiling protons in the angular range $61.2 - 77.4^\circ$ are sorted

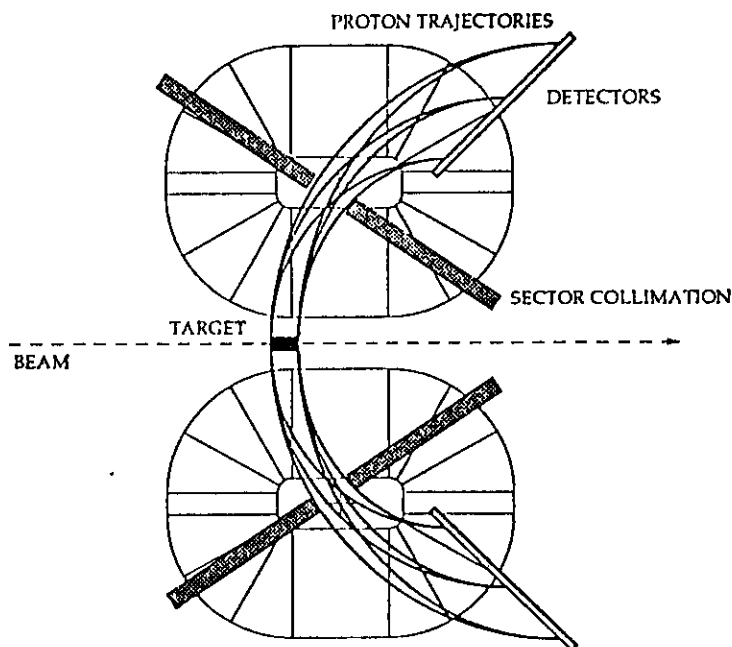


Figure 6: Schematic layout of the forward angle experiment (proton detection).

according to their Q^2 by the spectrometer. This Figure may be viewed as 1/4 of the experiment – it shows the particle trajectories for two of the eight segments of the azimuthally symmetric (with respect to the beam axis) spectrometer. With an incident energy of 3.0 GeV, this angular range for the protons corresponds to the Q^2 range of 0.1 – 0.55 GeV². Therefore, the forward angle asymmetries for the Q^2 bins centered at 0.125, 0.2, 0.3, 0.4, and 0.5 GeV² may be measured simultaneously by using segmented detectors. The protons are detected by an array of plastic scintillators which are nominally 1 cm thick. The detectors will be shielded from the target by the internal collimator (shown schematically) as well as by a much thicker lead shield for neutrons (not shown), and from general hall background with concrete shielding.

The layout for the backward angle measurement is similar except that the spectrometer is reversed with respect to the beam direction as shown in Figure 7. In this case electrons scattered from the (same) target cell are detected in the angular range centered around approximately 108°. For the backward angle measurements, the Q^2 range for a particular incident energy is small (typically 0.02 GeV²); therefore, each value of Q^2 requires a separate measurement at a specific incident energy. Four such measurements are planned corresponding to Q^2 values of 0.2, 0.3, 0.4 and 0.5 GeV² (the back angle asymmetry at $Q^2 \cong 0.1$ GeV² is being measured in the SAMPLE experiment at MIT-Bates). This setup will also be used to measure the asymmetry in quasielastic scattering from the deuteron to investigate the radiative correction associated with the axial- vector form factor (see Section 2.6).

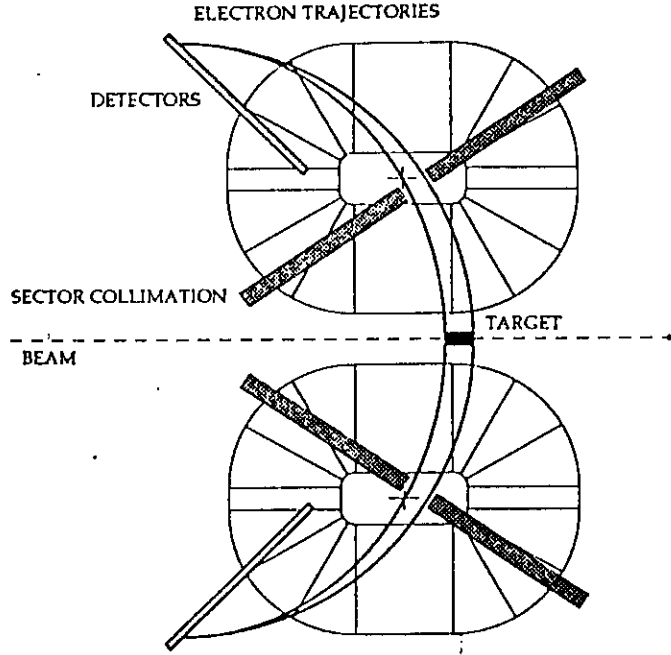


Figure 7: Schematic layout of the backward angle experiment (electron detection).

Table 3: Range of kinematics for forward angle asymmetry measurement (proton detection). The incident beam energy is 3.0 GeV.

Q^2 (GeV ²)	θ'_p (deg)	p' (MeV)	T'_p (MeV)	ϵ
0.10	77.4	321	53	0.994
0.55	61.2	797	293	0.962

The detailed kinematics for the experiment are presented in Tables 3 and 4. We note again that the forward angle asymmetries in five Q^2 bins will be measured simultaneously utilizing a beam energy of 3.0 GeV. Each Q^2 point at backward angles will require a different beam energy as shown in Table 4. The deuterium quasielastic measurement will likely be done at $Q^2 = 0.5$ GeV²; the kinematics are identical to the kinematics for elastic scattering from the proton at $Q^2 = 0.5$ GeV².

A summary of the experiment parameters is presented in Table 5. With the 20 cm LH₂ target (length limited by the spectrometer acceptance) and a beam current of 40 μ A (taking the same average current and hence the same beam power deposition density as in the SAMPLE experiment at MIT-Bates) the luminosity is 2.1×10^{38} cm⁻² s⁻¹. The beam will be rastered over an area of approximately 0.2 cm².

Table 4: Kinematics for backward angle asymmetry measurements (electron detection). A separate measurement (incident energy) is required for each Q^2 . The quasielastic deuterium experiment would likely be done at $Q^2 = 0.5 \text{ GeV}^2$ (the kinematics for the elastic proton and quasielastic deuteron are identical).

Q^2 (GeV^2)	E_k (MeV)	E'_k (MeV)	θ'_k (deg)	ϵ
0.2	335	228	108	0.200
0.3	428	268	108	0.196
0.4	512	299	108	0.192
0.5	590	324	108	0.188

Table 5: Experimental apparatus parameters.

Average current	$40 \mu\text{A}$
Target length	20 cm
Target thickness	1.4 g/cm^2
Luminosity	$2.1 \times 10^{38} \text{ cm}^{-2}\text{s}^{-1}$
Spectrometer acceptance (forward)	0.9 sr ($[\sin\theta\Delta\theta = 0.26, \Delta\phi = 0.45] \times 8$)
Spectrometer acceptance (backward)	$0.5 - 0.9 \text{ sr}$ ($[\sin\theta\Delta\theta = 0.15 - 0.26, \Delta\phi = 0.45] \times 8$)

Table 6: Summary of rates, asymmetries and uncertainties for the forward angle measurement.

Q^2 (GeV ²)	$\Delta\Omega'_p$ (sr)	$d\sigma/d\Omega'_p$ ($\mu\text{b}/\text{sr}$)	Rate (MHz)	A (10 ⁻⁶)	Time (h)	ΔA_{stat} (10 ⁻⁷)	$\Delta A_{stat}/A$ (%)
0.10 - 0.15	0.155	1.19	38.7	-3.06	700	2.07	6.8
0.15 - 0.25	0.239	0.671	33.7	-4.76	700	2.21	4.7
0.25 - 0.35	0.187	0.283	11.1	-8.90	700	3.86	4.3
0.35 - 0.45	0.155	0.146	4.75	-13.9	700	5.90	4.2
0.45 - 0.55	0.134	0.0850	2.39	-19.4	700	8.32	4.3

The rates, asymmetries and statistical uncertainties for the forward and backward angle measurements are presented in Tables 6 and 7. The rates given are for the entire spectrometer. Each of the eight segments will be instrumented with 14 plastic scintillator detectors – the segmentation being necessary to maintain a maximum counting rate of 1 MHz in each detector. We note that for the backward angle measurement typically one to four detectors per segment will be required to measure the elastic electrons (inelastic electrons can be measured in the other segments which correspond to lower momentum). The asymmetries in these Tables are calculated assuming no s quark contribution. The running times are chosen to obtain roughly 5% statistical precision. A 3% measurement is required for the deuterium quasielastic measurement; because of the larger cross section and asymmetry this measurement requires a shorter running time. A beam polarization of 49% is assumed throughout.

3.3 Physics backgrounds

3.3.1 Introduction

In the forward angle measurement the spectrometer described in the Technical Design Report will accept protons over a broad but correlated range of momenta and scattering angles corresponding to the recoil proton kinematics. For the forward angle measurement the main backgrounds come from inelastic protons and pions. The backward angle measurement should be very clean since π^- 's are kinematically forbidden and there is a significant separation between elastic and inelastic electrons.

Table 7: Summary of rates, asymmetries and uncertainties for the backward angle measurements. The deuterium quasielastic measurement is shown in the last line of the table. It requires less time to obtain a smaller relative uncertainty in the asymmetry both because the cross section and asymmetry are larger than those for the proton measurements.

Q^2 (GeV ²)	$\Delta\Omega'_k$ (sr)	$d\sigma/d\Omega'_k$ (nb/sr)	Rate (MHz)	A (10 ⁻⁶)	Time (h)	ΔA_{stat} (10 ⁻⁷)	$\Delta A_{stat}/A$ (%)
0.2	0.9	41.2	4.33	-12.3	390	6.18	5.0
0.3	0.75	22.4	2.43	-19.6	470	8.25	4.2
0.4	0.6	13.6	1.43	-27.6	580	10.8	3.9
0.5	0.5	8.84	0.928	-35.4	700	13.3	3.8
0.5	0.50	12.2	1.28	-47.2	460	14.0	3.0

3.3.2 Inelastic protons

Two studies have been made of the inelastic proton background for the forward angle measurement. First, a measurement was carried out at SLAC using the NPI injector beam at 2.4 GeV and the 1.6 GeV spectrometer at a scattering angle of 63.5°, essentially the same kinematics as for the proposed experiment. While this measurement was not made under ideal conditions (the spectrometer trigger was set up for positrons, with pions and protons being prescaled by a factor of 128, and all the measurements were made in about 30 min), the results support the inelastic cross sections from the Lightbody and O'Connell code as shown in Figure 8. The data in this Figure correspond to only the elastic and inelastic protons. The pions have been (largely) cut out using a pulse height cut on the scintillators. The background that extends above the elastic peak might be pions that were not excluded by the cut (we note that the elastic peak energy is the kinematic limit for inelastic protons from the LH₂ in the target). There were no positrons seen, with a limit of about 10⁻⁴ of the elastic proton rate.

Whereas the momentum and scattering angle resolution of the 1.6 GeV spectrometer in the above case are relatively very good, the spectrometer in the the present experiment has poorer resolution but is tightly correlated to the elastic kinematics. A detailed Monte Carlo study has been performed using the inelastic proton cross sections from Lightbody and O'Connell, and including the optics parameterization of the spectrometer for the full acceptances as well as multiple scattering in a realistic target. This Monte Carlo also includes the cut from the collimator in the middle of the spectrometer (also described in the Technical Design Report, Section 8.3.5). It should be noted that whereas the coils of the spectrometer enclose a large volume, the restriction of the allowed phase space at the

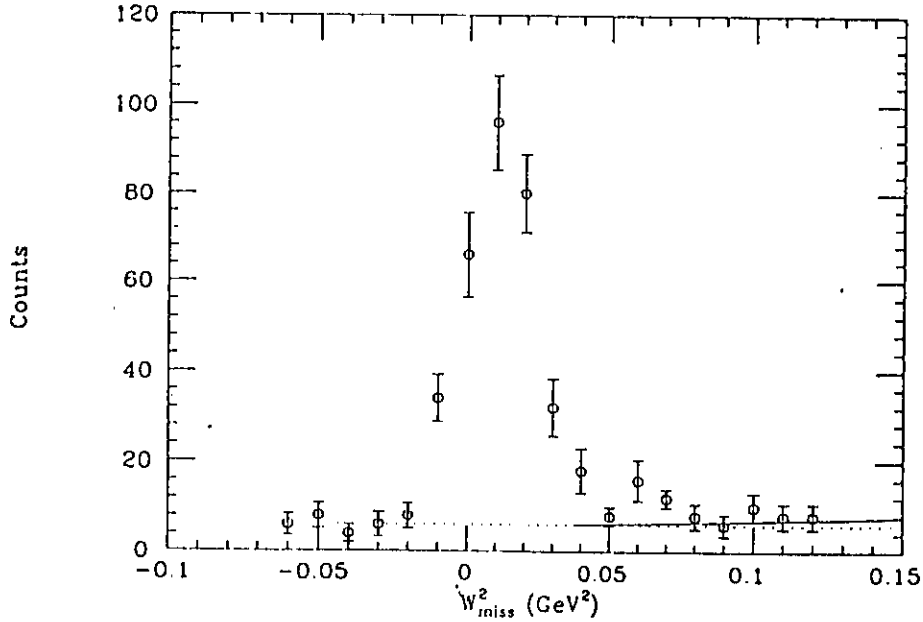


Figure 8: Proton spectrum from elastic ep scattering at 2.4 GeV incident energy and proton scattering angle of 63.5° . The calculation of the inelastic protons (solid line) is from the code of Lightbody and O'Connell. The residual background (dotted line) seen above the peak may be due to π^+ that were not cut from the spectrum.

focal plane represented by the collimator is very severe. In other words, this is not an open spectrometer geometry like that of the CLAS, but is more nearly like that of the 1.6 GeV from the point of view of shielding of the detectors. The Monte Carlo results for the (combinations of) detector segments corresponding to each Q^2 bin are shown in Figure 9.

The ratios of the raw (no time-of-flight cut) inelastic background to the elastic signal are listed in Table 8. These ratios can be reduced by applying a time-of-flight cut; at $Q^2 = 0.3 \text{ GeV}^2$ such a cut reduces the background by a factor of about two. The t.o.f. spectrum for this typical case is shown in Figure 10. Finally, by simultaneously measuring the inelastic asymmetry using the appropriate time bin, the uncertainty in the contribution of the inelastic protons to the elastic asymmetry should be reduced to negligible levels.

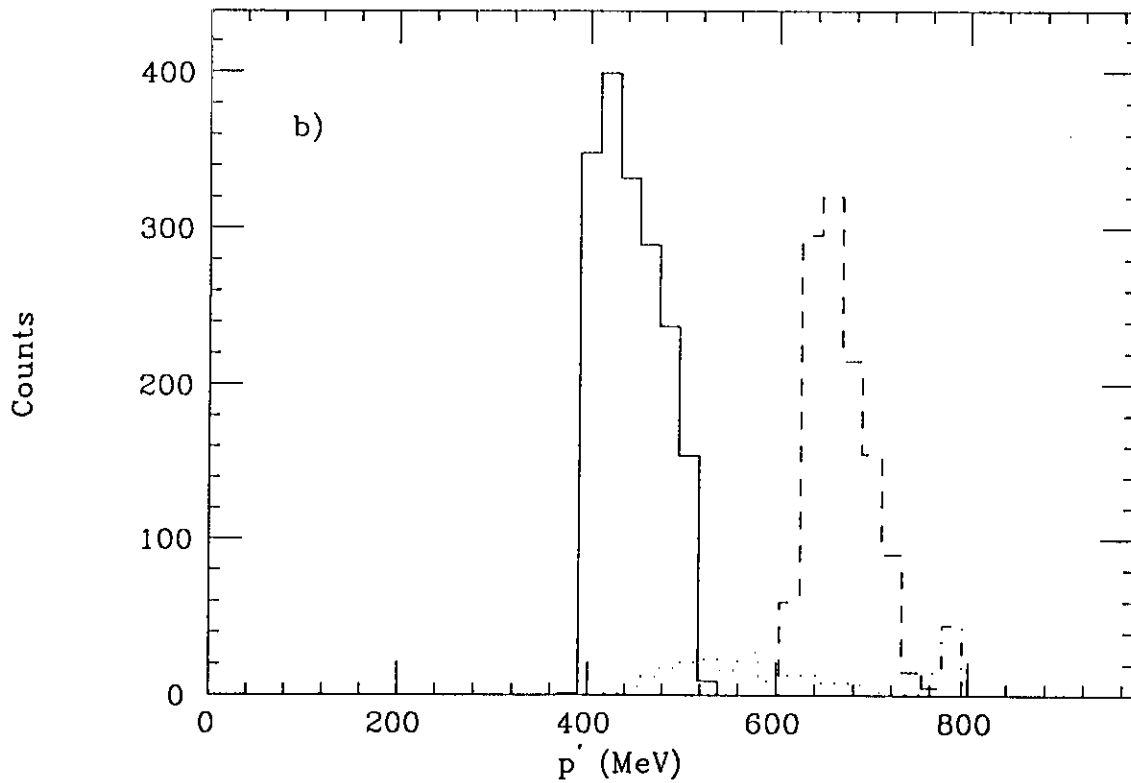
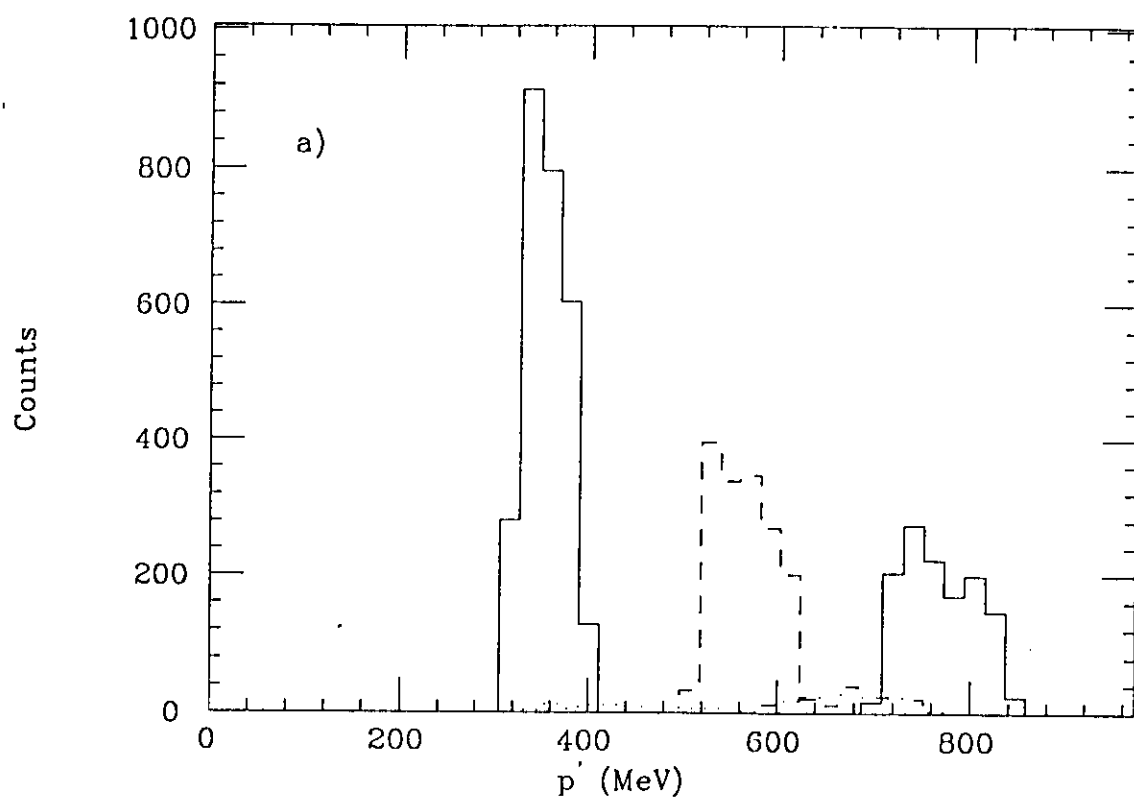


Figure 9: Monte Carlo simulation of elastic (inelastic) proton spectra for detector segments corresponding to a) $Q^2 = 0.125$ solid (dotted) histogram, $0.3 - \times 3$ - dashed (dotdashed) histogram and $0.5 \text{ GeV}^2 - \times 10$ - solid (dotted) histogram, and b) $Q^2 = 0.2$ solid (dotted) histogram and $0.4 \text{ GeV}^2 - \times 5$ - dashed (dotdashed) histogram.

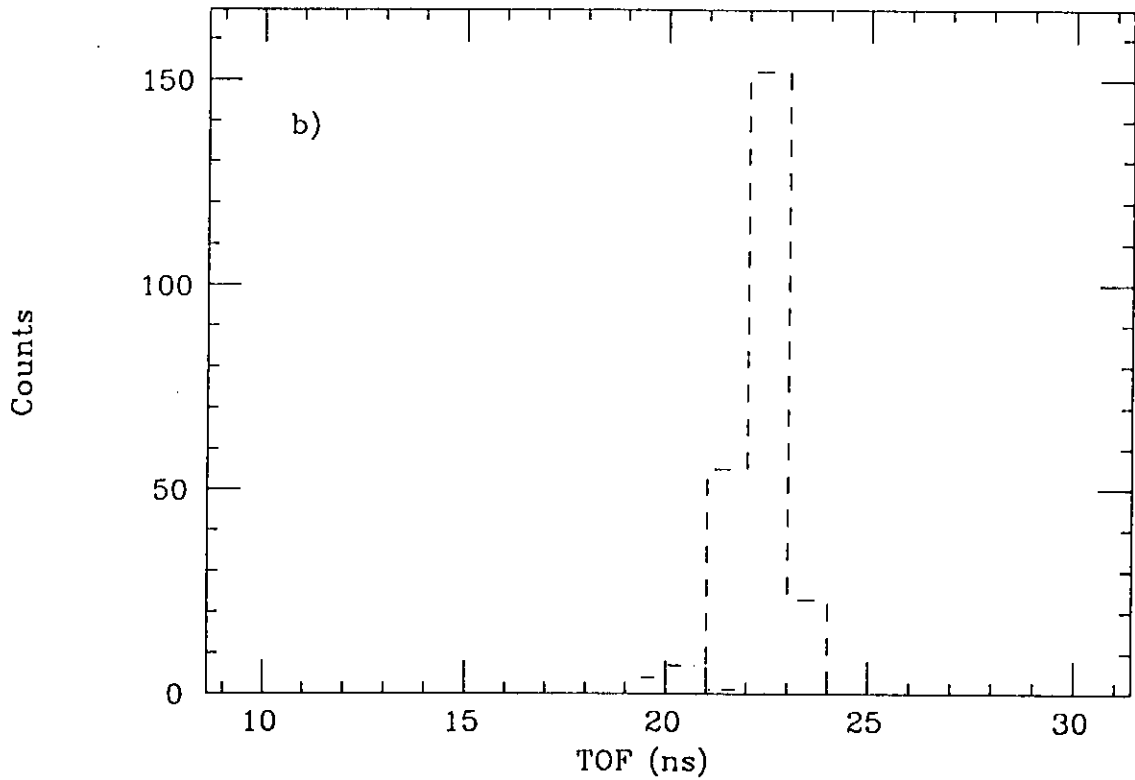
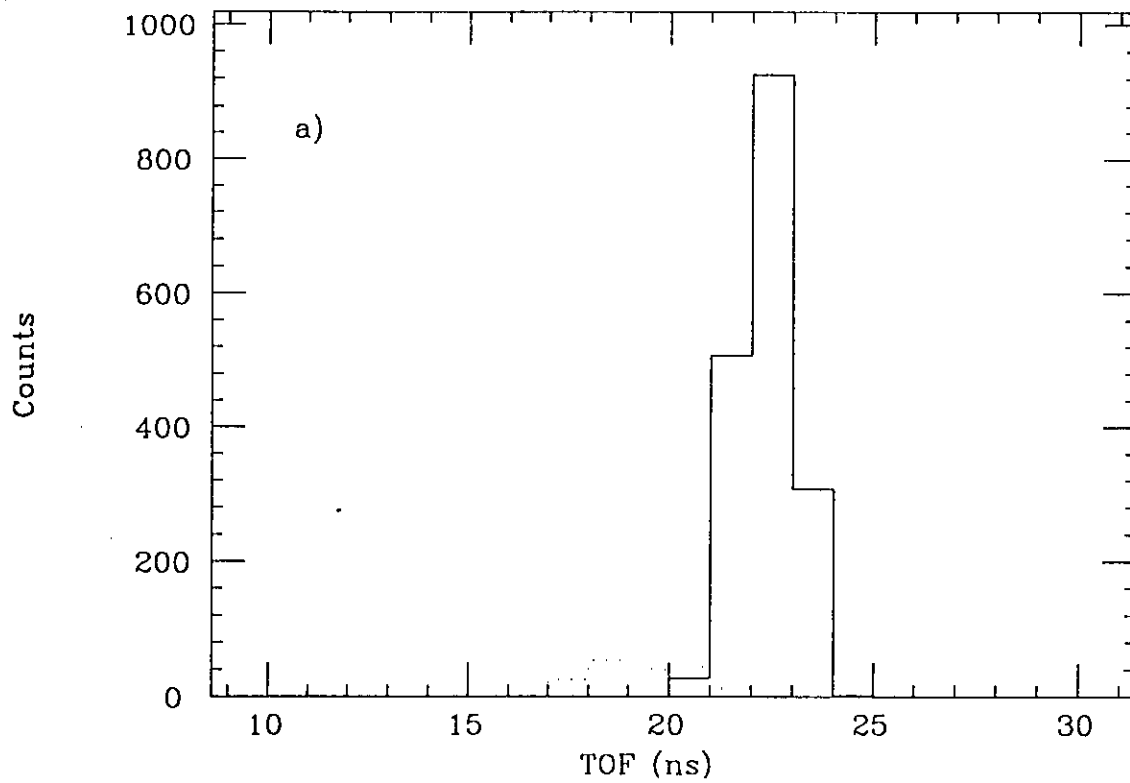


Figure 10: Time-of-flight spectra for protons at a) $Q^2 = 0.2 \text{ GeV}^2$ and b) $Q^2 = 0.4 \text{ GeV}^2$.

Table 8: Ratio of raw (i.e. no time-of-flight cut) inelastic to elastic protons, \mathcal{R}_{inel} for each Q^2 bin.

Q^2 (GeV ²)	\mathcal{R}_{inel} (%)
0.125	3.4
0.2	9.9
0.3	11.2
0.4	5.2
0.5	< 0.5

3.4 Neutrons

The high luminosity required for this experiment will result in a high rate of neutron production in the target. If left unshielded, these would cause high background rates in the scintillation counters. In addition to degrading the performance of these counters, this would tend to dilute the asymmetry. Furthermore, if there is a helicity dependence to the neutron production, this would contaminate the asymmetry of interest. Heavy shielding will surround the spectrometer to reduce 'room background' neutrons from external sources, such as the beam dump. Because of its close proximity to the detectors, shielding of the target merits special attention. The emphasis will be placed on the line-of-sight between the target and detectors. Neutron shielding will be built into the spectrometer to reduce this background to inconsequential levels. No attempt will be made to block the most intense flux of neutrons, at small angle from the beam, so as to avoid scattering them into the detectors.

A first-iteration design for the shielding has been tested using a standard neutron simulation Monte Carlo code, MCNP [LA81], with a well-tested high energy transport front-end, LAHET [Pr89]. Several enhancements of the code were required to make the source and detection descriptions suitable for this task. An elongated source was added, with the actual starting point of each neutron randomly chosen along a 20.0 cm length to simulate the effect of the finite length of the target. The initial energy of each neutron is chosen randomly, according to a weighting distribution, and the initial angle is then chosen with a weighting distribution appropriate for that energy. In both cases the distributions used are simple parameterizations of experimental distributions for protons observed in inelastic electron scattering at several GeV incident electron energy. The approximation is made that the inelastic neutron cross-section is equal to that for protons. Finally,

detection probability is modeled by a reasonable mean free path applied to the actual detector thickness presented to each neutron. This is determined from the angle (relative to the normal) of each neutron as it crosses the detector surface, which is presently modeled as sections of a cone.

Figure 11 shows a cross-sectional view of the present shield simulation. The shield has rotational symmetry about the beam axis, forming a cone, except for gaps at the positions of the spectrometer's super-conducting coils. The first layer encountered by the neutrons is made of lead and has a central thickness of 41 cm along the flight direction. This serves to scatter some neutrons off the path to the detector and to degrade the energy of most of the remainder. This is followed by 25 cm of paraffin and boraffin (borax-doped paraffin) to slow and absorb the neutrons. Early calculations showed that the shield itself acted as a significant source of low energy background neutrons in the diametrically opposite detectors. A 2 cm thick paraffin backing has been added on the beam-side of the detectors to protect against this effect. The lead shield is not a rectangle in cross-section because our studies have shown that the inner corner would then act more as a source of neutrons than as an effective shield because of the high flux of small-angle neutrons which would strike it.

The rates of above-threshold neutron-induced interactions calculated in this model vary across the focal plane from about 16 kHz to 40 kHz per detector. Of this, about 6 kHz results from neutrons penetrating the shield and the majority of the remainder results from neutrons which are scattered from the shield into another detector, not along the original line of sight. The next stage of the optimization is clearly to try to eliminate those neutrons which are scattered out of the line-of-sight shielding toward other sectors. This can be accomplished by simply increasing the thickness (presently only 2 cm) of the paraffin backing near the detectors. The goal is, therefore, to try to approach the neutron rate from direct penetration.

These rates are quite moderate in comparison to the average 500 kHz signal rate expected when the spectrometer is in this forward-angle configuration. In addition, because of the wide range of speeds and flight-paths involved, the neutrons are expected to be roughly uniformly spread in time. The proton signal of interest is expected to come within a window of approximately 3 ns out of the 32 ns repetition time. The contamination of the signal by neutrons will thus be decreased by an order of magnitude by the time-of-flight cut. This should reduce the neutron contribution under the peak to a few percent or less of the signal, with the present shield design. The effect of dilution of the measured asymmetry will therefore be small and calculable. (It will be possible to estimate neutron background contribution both by interpolation of the flat background and by measuring rates with the spectrometer field off.) The false asymmetry contribution should also be small, even if the asymmetry of the neutron background is several times larger than the

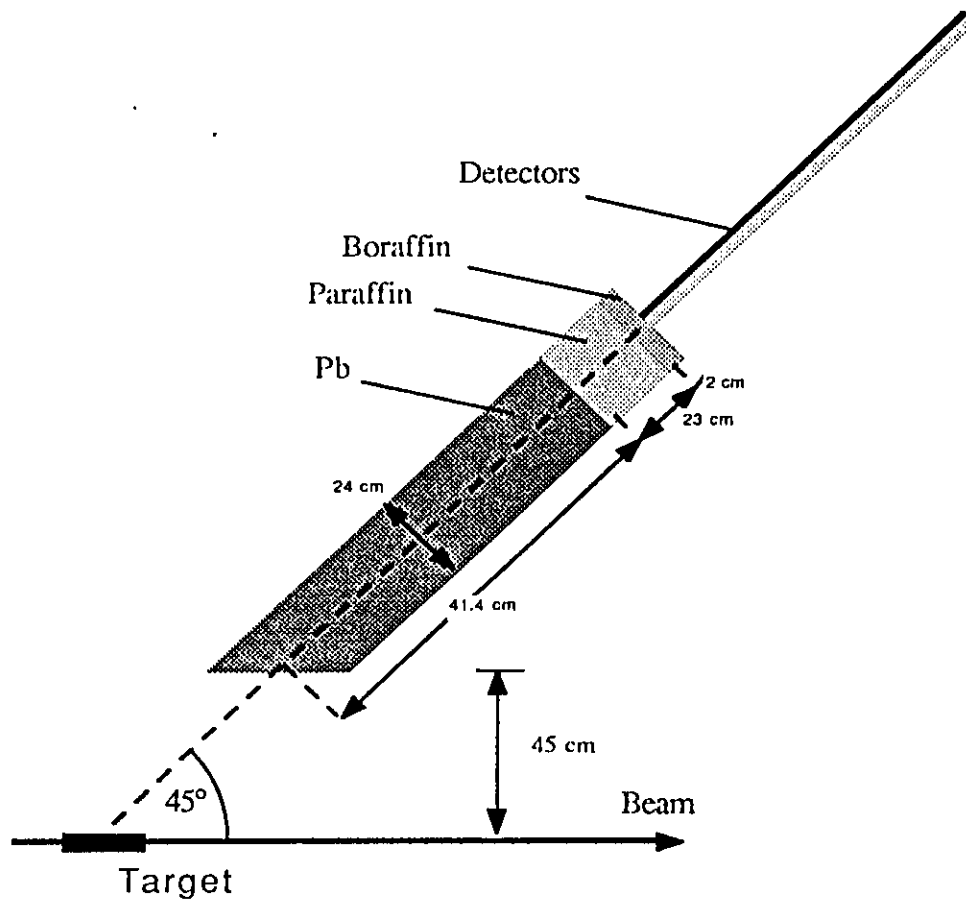


Figure 11: Cross-sectional view of the simulated neutron shield. Shield has rotational symmetry about the beam, except for eight 12 cm gaps at the positions of the magnet coils.

asymmetry of interest.

Further studies of the neutron background and optimization of the shielding are continuing, using the Monte Carlo programs described above.

3.4.1 Pions

For the forward angle measurement, the π^+ background, dominated by pions from Δ production at relatively low Q^2 (effectively from photoproduction), is essentially independent of momentum and angle in the acceptance of the spectrometer (cross sections from the code of Lightbody and O'Connell [Li88]). The rate in each detector is roughly equal to the elastic rate at $Q^2 = 0.4 \text{ GeV}^2$. These pions (and any other prompt particles that evade the shielding) are easily discriminated using time-of-flight (typically 6 ns as compared with roughly 20 ns for the protons) and/or scintillator pulse height (using a threshold discriminator); if they are not cut out by the discriminator their asymmetry can be measured simultaneously by recording the information from the appropriate time bin. Since there is no direct contribution of these pions to the elastic proton signal, the only effect will be on the dead-time. However, the difference in pion rate for positive and negative helicity electrons is at most on the order of that of the protons, hence, since the dead-time is small (about 0.03 counts maximum per detector in each machine period of 32 ns), the effect on the proton asymmetry will be negligible.

Production of π^- is kinematically forbidden at the low incident energies required for the back angle measurements (because production of two pions is necessary). If measurements of higher Q^2 back angle asymmetries are pursued, π^- contamination of the elastic electron signal can be sufficiently reduced using relatively small aerogel Čerenkov detectors to back the scintillators covering the elastic acceptance (the elastic rates in these cases are 10's of kHz at most).

3.4.2 Inelastic electrons

The backward angle measurements of electrons will essentially be free of background contamination. There is a significant energy gap between the elastic electrons and those inelastic electrons at the pion production threshold. Figures 12 and 13 show the separation of the elastic and inelastic events for measurements at $Q^2 = 0.2$ and 3.0 GeV^2 with effective solid angle acceptances of 0.9 and 0.28 sr, respectively. Since, unlike the recoil protons in the forward angle measurement, the elastically scattered electrons are in this case contained on a few detectors, the inelastic background and its asymmetry may be measured simultaneously with the separate detector elements corresponding to lower

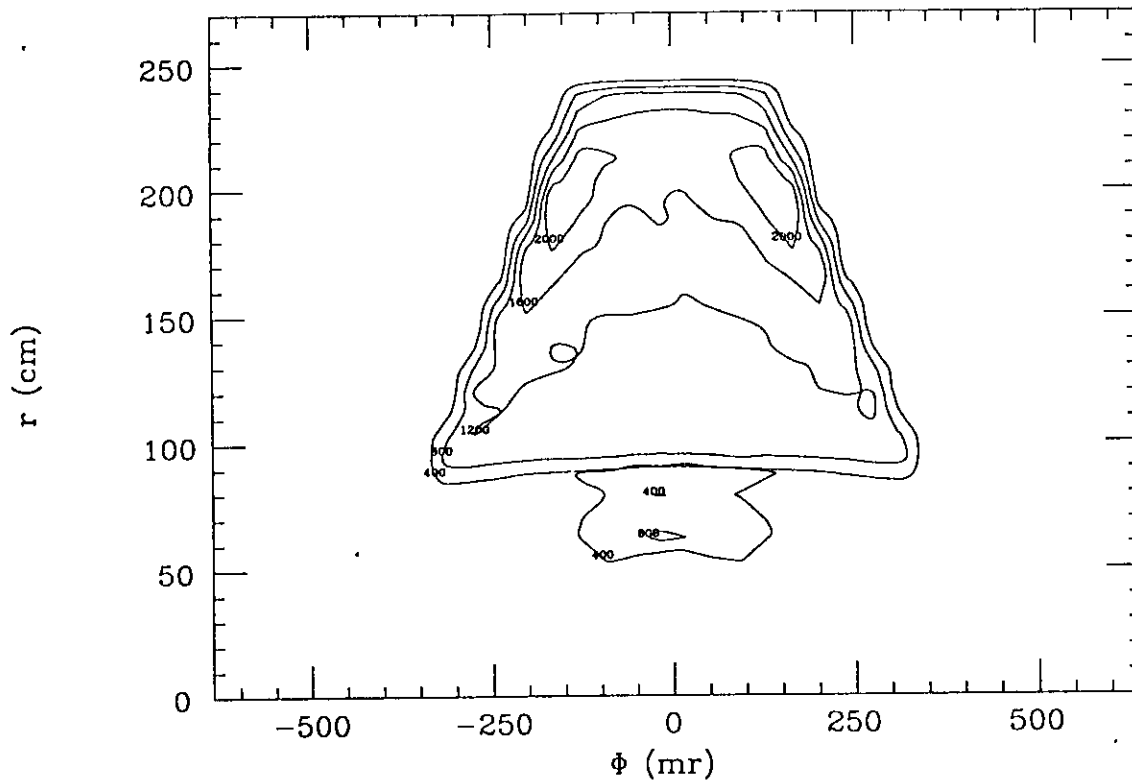


Figure 12: Monte Carlo simulation of elastic (upper) and inelastic (lower) electron spectra for $Q^2 = 0.2 \text{ GeV}^2$. R and Φ are defined in the Technical Design Report, Section 8. For the $Q^2 = 0.2 \text{ GeV}^2$ simulation the current in spectrometer is reduced to 50% of its nominal value.

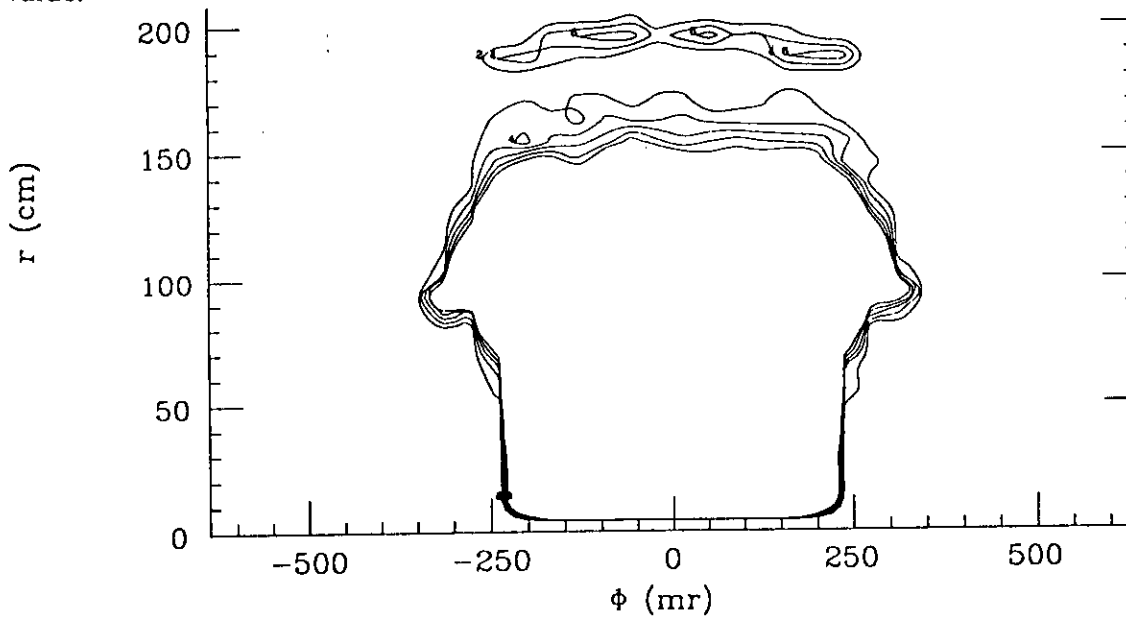


Figure 13: Monte Carlo simulation of elastic (upper) and inelastic (lower) electron spectra for $Q^2 = 3.0 \text{ GeV}^2$. R and Φ are defined in the Technical Design Report, Section 8. Contour interval for elastic (inelastic) events is 2(4) counts.

momenta. The neutron background, which will again be approximately uniform over the interval between beam pulses, is expected to be a factor of about two smaller than in the forward angle measurement [De68].

The separation of elastic, quasielastic and inelastic electrons in the deuterium measurement should be possible with an acceptance of 0.5 sr since the separation in energy of the elastic and quasielastic peaks is larger than that of the quasielastic peak and the pion production threshold. Again the yield and asymmetry of the elastic and inelastic electrons may be measured concurrently using detectors on either side of that containing the quasielastic peak. It is possible in this case that detectors (covering a relatively small area of the focal plane) would have to be replaced with (or backed up by) Čerenkov detectors to reject the small π^- background from (neutron) resonance decay (the kinematic limit for π^- is just below the quasielastic electron energy).

3.5 Room shielding

In addition to the internal shielding in the spectrometer used to restrict the angular acceptance (collimators), prevent particles further from the angular acceptance from reaching the detectors, and scatter line of sight neutrons away from the detectors, there will be approximately 1m of concrete shielding surrounding the detectors as outlined in the Technical Design Report, Section 9.13. An equivalent thickness of shielding will be required to shadow the switchyard tunnel exit into the hall.

3.6 Compatibility with other Hall C experiments

As discussed in the Technical Design Report, Section 9.13, when the G0 spectrometer is on the beamline the angular range of the HMS is unaffected and that of the SOS is restricted to $\theta_{SOS} \lesssim 135^\circ$. There are presently no approved or conditionally approved experiments which would use the SOS at angles greater than 135° .

The simplest possible scenario for G0 operation is to simply remove the hydrogen from the target cell and move it off the beamline. This general capability exists presently in the SAMPLE target; it is straightforward to extend the range of motion by a sufficient amount. The target could also be warmed and removed by withdrawing it from the spectrometer through an 'airlock'. Lastly, the spectrometer will be able to move in and out of the beamline (while cold) on Hillman rollers or airpads. This option allows maximum flexibility for the beamline and unrestricted motion of the SOS.

The standard Hall C beamline from G0 downstream including the scattering chamber

will be removed for operation of this experiment. We plan to continue the beamline vacuum from the spectrometer to just downstream of the standard pivot where the He bag begins with large aperture beam pipe.

4 Asymmetry Measurement Methodology

4.1 Introduction

Because parity-violating asymmetries are small, analysis of the data in this experiment is more involved than in other electron scattering measurements. However, the framework is relatively straightforward. The starting point for assessing the uncertainties in the asymmetry is the normalized yield, i.e. the number of counts in the detector per unit beam charge. The asymmetry is determined from yields for the two beam helicities (each measured for a time T_h):

$$A^{meas} = \frac{Y_+ - Y_-}{Y_+ + Y_-}$$

where

$$\begin{aligned} Y_h &= \frac{(d\sigma/d\Omega)\mathcal{L}\Delta\Omega T_h}{Q_h} \\ &= \frac{C_h}{Q_h} \end{aligned}$$

and $d\sigma/d\Omega$ is the differential ep cross section, \mathcal{L} is the luminosity, $\Delta\Omega$ is the solid angle acceptance, and C_h and Q_h are the total number of counts in the spectrometer and the beam charge passing through the target in time T_h , respectively. In each signal used to determine these quantities there may be, in addition to the true signal, contributions from random (not correlated with beam helicity) background noise, helicity correlated background noise and helicity correlated changes in beam, target and/or detector properties. The helicity correlated piece is separated into the set which can, in principle, be corrected, and the remainder (“correlated noise”). These contributions comprise the uncertainties and corrections for the experiment and are examined in turn below. Assessment of these contributions leads to tolerances on various parameter measurements (for example, beam position) as well as to a framework for data taking.

The experiment will involve both the counting of individual scattered protons and electrons as well as the integration of various signals from beam monitors. Those systematic effects which can be corrected enter the two types of measurements in similar ways; the effects of noise enter in different ways. These considerations are detailed below.

For the purpose of planning the experiment, in order to obtain a consistent set of specifications, the following criteria have been adopted uniformly in the following material. For individual contributions to both statistical and systematic uncertainties the goal is set at 5% of the overall goal for the experiment. For example, individual false asymmetries should be less than $5\% \times 2.5 \times 10^{-7} \cong 1 \times 10^{-8}$.

The remainder of this section is organized as follows. First, the data-taking time sequence is described. The statistical and systematic uncertainties are then discussed. Lastly, the analysis scheme for an asymmetry with background is presented.

4.2 Data-taking sequence

The overall experiment timing diagram is shown in Figure 14. In order to measure proton time-of-flight in the forward measurement, every 16th micropulse of the nominal 500 MHz Hall C pulse train is used. We expect that this will be accomplished using a mode-locked laser operating at 31.25 MHz (see the Technical Design Report, Section 5).

The unit of measurement time for the experiment ('the measurement interval' or 'macropulse'), T_h , will likely be 1/30 s to reduce the effect of 60 Hz (plus harmonics and subharmonics) noise as much as possible (see also Section 4.3.2). The helicity of the beam therefore remains constant for this period. For the time Δt (presently estimated to be $\leq 100 \mu\text{s}$) after the measurement interval of 1/30 s, the master data-taking gate for the experiment will be disabled while the beam helicity is flipped and the beam monitors are read out. The beam (running at 31.25 MHz) continues throughout. The beam helicities will be randomly chosen patterns of four, $+ - - +$ or $- + + -$, such that the average time of measurement of $+$ and $-$ helicity for each set is the same. The asymmetries will then be calculated for each set of four. Long term drifts that are essentially linear over these 4/30 s intervals will not effect the asymmetry measurement as a result (see also Section 4.3.2).

In addition to these time scales, the beam will be "rastered" on the target to reduce the local power density. We anticipate covering an area of about 0.2 cm^2 , consistent with the design for the SAMPLE experiment. The horizontal and vertical rastering coils, operating at about 10 kHz, will be driven at slightly different frequencies to produce a Lissajous figure on the target cell. The rastering pattern will be the same for each measurement interval.

4.3 Statistical uncertainties

4.3.1 Beam charge measurement

The uncertainty in the measurement of the charge should contribute only a small amount to the overall uncertainty in the asymmetry, i.e. it should be significantly smaller than the uncertainty in the spectrometer signal. The uncertainty in the charge measurement will be dominated by uncorrelated background noise (i.e. not particle counting statistics) to be discussed in general in Section 4.3.2. For all uncorrelated noise contributions to the

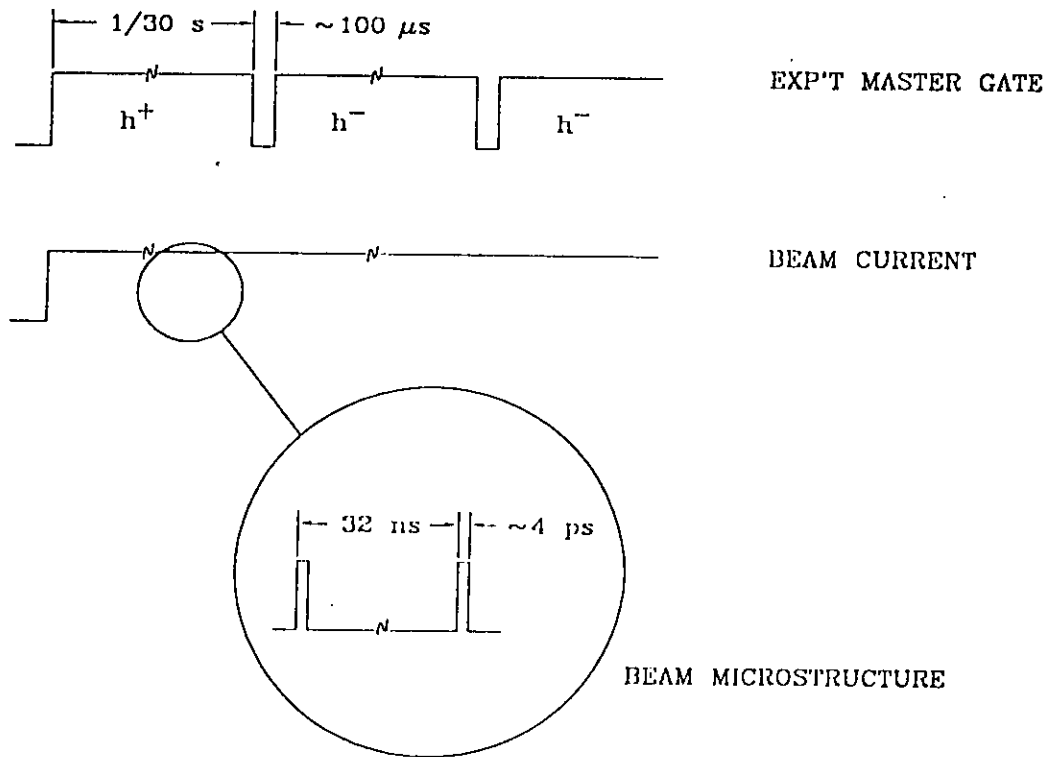


Figure 14: Overall experiment timing diagram. The beam is pulsed at 31.25 MHz; the basic measurement time will be $T_h = 1/30$ s. Times between measurement intervals when beam helicity is flipped and the experimental equipment is read out is $\delta t \lesssim 100 \mu s$; the beam runs continuously throughout.

overall uncertainty, the goal in this proposal is taken to be 5% of the uncertainty due to counting statistics (for the case of the highest counting rate of $\sim 40\text{MHz}$ for the low Q^2 bins in the forward angle measurement). Therefore, if the measurement time is taken to be $T_h = 1/30$ s (as it will be throughout for illustration) the relative uncertainty required in the charge measurement is 5% of the relative uncertainty in the number of counts in time T_h , i.e.

$$\begin{aligned}\frac{\Delta Q}{Q} &= 0.05 \frac{1}{\sqrt{40 \text{ MHz } T_h}} \\ &= 4 \times 10^{-5}.\end{aligned}$$

Note that consideration of the helicity correlated beam intensity changes yields the same tolerance as will be discussed below. With modest improvements in existing r.f. cavity charge monitors we hope to meet this objective (see the Technical Design Report, Section 6.4).

4.3.2 Uncorrelated background noise

In this section the general effects of noise not correlated with beam helicity are considered and a measurement strategy is developed to reduce them to as low a level as possible. The effects in the counting and integration modes are similar; the result in either case is that if the background is small relative to the signal in each measurement (of duration T_h), it will remain so in the final result if some simple precautions are taken. In the following the measured signal is denoted by S , the true (real) signal by R and the uncorrelated background by B .

In a measurement of duration T_h (with a single beam helicity), the overall uncertainty will be

$$\Delta^2 S = \Delta^2 R + \Delta^2 B$$

where $\Delta^2 R = C_h$ in the case of the signal from the spectrometer. If the true signal is to be measured very precisely using N such measurement intervals, then as long as two conditions are fulfilled the resulting uncertainty will be dominated by that of R . First, $\Delta^2 B$ must be smaller than $\Delta^2 R$, and, second, the N time intervals must be chosen in a random fashion relative to the background noise (in a sense that will become clear below) to prevent unintended helicity correlations. If these conditions are met, even if there is a significant background signal at, for example, a frequency of 60 Hz, $\Delta^2 S/S^2$ can in principle be made arbitrarily small (reduced by the factor N for many measurements).

In practice, to reduce the uncorrelated background as much as possible the following strategy will be used (as outlined briefly in Section 4.2). First, measurements will be

made for the period T_h corresponding to a frequency $f_h = 1/T_h$. (Note that while each measurement interval will be precisely T_h , the beam helicity will be changed with a period of $T_h + \delta t$ where the time $\delta t \lesssim 100 \mu\text{s}$ is used to change the helicity and read out the electronics after each measurement). This frequency will likely be 30 Hz depending on whether this is a quiet region of the local power spectrum of uncorrelated noise. For this discussion it is assumed that $f_h = 30 \text{ Hz}$. Second, suppose that the pattern of four beam helicities $+ - - +$ is used for four consecutive measurement intervals and suppose this pattern or its complement is chosen randomly to make up the N measurements. The uncorrelated noise components with frequencies $f \gg f_h$ will largely average to zero leaving some small residual which will be reduced by N as in the preceding paragraph. Background components with frequencies at harmonics of 30 Hz will be averaged to zero with high precision in each measurement interval t_h . For background components with frequencies $f \ll f_h$ (for example, long term drifts), averaging measurements from intervals one and four, and two and three (i.e. the averaged measurements for each helicity are effectively made at the same time) before forming the asymmetry will result in cancellation of the effect of these low frequency components to the extent that they are changing linearly over the time period $4T_h$. For frequencies closer to f_h (where little power is expected), the contributions will simply be reduced by making N measurements as above. Note that if the $+ - - +$ and $- + + -$ patterns were not chosen randomly, noise at a frequency of $f_h/4$ would accumulate, generating an unintended helicity correlation.

The effect of uncorrelated noise in an integrated signal is straightforward - it simply adds to the true signal. In the counting mode, noise may enter, for example, the double pulse resolution time (i.e. this resolution may fluctuate). The true number of counts in a measurement interval C_h is

$$\begin{aligned} C_h &= M_h + lM_h \\ &= M_h(1 + r\tau_d) \end{aligned}$$

where M_h is the measured number of counts and the loss fraction l is product of the rate r and the double pulse resolution time τ_d . The uncertainty in C_h is then

$$\Delta^2 C_h = \Delta^2 M_h (1 + r\tau_d)^2 + M_h^2 r^2 \tau_d^2 \frac{\Delta^2 \tau_d}{\tau_d^2}$$

i.e., it has a piece from ordinary counting statistics and a piece due to uncorrelated noise in the double pulse resolution time τ_d (the rate, unlike the double pulse resolution, is measured in the course of the experiment). For this experiment if the noise due to double pulse resolution fluctuations is to be less than 5% of the overall uncertainty, with loss fractions of 3% the relative fluctuations (over the period $4T_h$) in the double pulse resolution (averaged over eight detector elements) must be less than about 1×10^{-3} . (The noise in

question here is the residual noise, i.e. that noise not eliminated by the data-taking methodology described above.)

There will be a similar noise contribution in time-of-flight measurements. For example, consider the effect of a short gate of duration $T_g \cong 1$ ns set for each detector during the time the elastic protons arrive (see the Technical Design Report, Section 11). If the machine is pulsed every 32 ns, in the standard measurement time of 1/30 s there will be $N_g = 1.04 \times 10^6$ such gates. The uncertainty in the measured number of counts including that from the fluctuating gate width will therefore be

$$\begin{aligned} \frac{\Delta^2 C_h}{C_h^2} &= \frac{\Delta^2 M_h}{M_h^2} + \frac{\Delta^2 T_l}{T_l^2} \\ &= \frac{\Delta^2 M_h}{M_h^2} + \frac{1}{N_g} \frac{\Delta^2 T_g}{T_g^2} \end{aligned}$$

where T_l ($\propto T_g$) is the live time. Therefore $\Delta T_g/T_g$ must be smaller than 4% (again averaged over eight detectors) to meet the "5%" standard.

4.4 Systematic uncertainties and false asymmetries

4.4.1 Beam polarization measurement

The measured asymmetry defined above is related to the physics asymmetry by

$$A^{mcas} = P_e A^{phys}.$$

Therefore the uncertainty in the average beam polarization adds to the other systematic uncertainties in the experiment. Differences in the polarization for the two helicity states will not be important (see Section 4.4.3). We expect to be able to measure the average polarization to 2% (see the Technical Design Report, Section 6.5).

4.4.2 Correlated background noise

There are many parameters throughout the entire experimental apparatus (including the accelerator) whose variations will be correlated with helicity at some level. The effects of those apparatus parameters which can be measured independently will be treated in below; variations in all other parameters will be seen only indirectly in the spectrometer (or charge monitor) signal. These effects are referred to here as helicity-correlated background noise. They can be distinguished by providing for different means of reversing the beam

helicity. For this experiment at least two different methods will be used. The “fast” helicity reversal will be effected by changing the sign on the drive signal of a Pockels cell “ \pm quarter-wave plate” in the laser drive for the source. In addition there is provision in the laser drive for the polarized source to insert a 1/2-wave plate in the optical path which will reverse the sign of the helicity at the target without any other changes (in particular, without changes in electrical signals) in the system. In practice this plate would be inserted for half the running time (changing from ‘plate in’ to ‘plate out’ several times during the experiment). The offset in the asymmetries so measured (which should only differ by a sign) is the overall effect of correlated noise on the asymmetry. Finally, the spin direction of the electrons in the beam can be changed to an arbitrary orientation using the electrostatic spin manipulator in the polarized source. Therefore, the polarization of the electrons upstream of the manipulator can be reversed in the normal way and the manipulator tuned to provide, for example, transverse polarization at the target in which case the parity-violating asymmetry effectively vanishes.

4.4.3 Corrections for correlated parameter variations

In the expression above for the normalized yield all terms are effected by one or more of the beam, target and spectrometer properties except for the measurement interval. Many of these properties can be measured independently of the main signals to determine their dependence on beam helicity. Specifically, the beam energy, position, angle, shape, polarization and intensity will be measured in addition to the relative acceptances of the detector elements. The response of the yield to variations in these parameters (the *measured* derivatives rather than the various derivatives *calculated* below will be used for the analysis) as well as their helicity dependence will be measured continuously throughout the experiment. The tolerances for these measurements are again determined here by requiring that the false asymmetry corresponding to the tolerance is less than 5% of the overall systematic uncertainty in the asymmetry. If the time interval considered for measuring these parameters is again taken to be $T_h = 1/30$ s, the corresponding uncertainty in the asymmetry is about 8×10^{-4} ; therefore, in 1/30 s the false asymmetry resulting from the resolution of the parameter measurements should be less than 4×10^{-5} .

In practice, each measured asymmetry A_m is composed of a number of such false asymmetries $A_{f,i}$ in addition to the true asymmetry A_t and the contribution from the correlated noise A_{cn} discussed in the previous section

$$\begin{aligned} A_m &= A_t + A_{cn} + \sum_i A_{f,i} \\ &\cong A_t + A_{cn} + \sum_i \frac{1}{Y} \frac{\partial Y}{\partial \alpha_i} \delta \alpha_i \end{aligned}$$

Table 9: Tolerances on beam and spectrometer parameter measurement. Measurements are all assumed to be made in the time period $T_h = 1/30$ s. The quoted values are all relative (measurement interval to measurement interval). The linear tolerance for the beam energy assumes a dispersion of 2.5 cm/%. The tolerances on the beam position and angle measurements depend on the relative efficiency of opposite detector pairs being corrected at the 5×10^{-3} level. The linear tolerance for the beam angle assumes two measurements 10 m apart.

Incident energy	1×10^{-5} (25 μm)
Beam diameter at target	1 mm
Beam charge	4×10^{-5}
Beam position at target	800 μm
Beam angle at target	14 μr (100 μm)
Detector asymmetry	5×10^{-3}

since for $Y_+ = Y_-$

$$\begin{aligned}
 A_{j,i} &= \left\{ Y_+ \left(1 + \frac{1}{Y} \frac{\partial Y}{\partial \alpha_i} \delta \alpha_i \right) - Y_- \left(1 - \frac{1}{Y} \frac{\partial Y}{\partial \alpha_i} \delta \alpha_i \right) \right\} \\
 &\quad \left\{ Y_+ \left(1 + \frac{1}{Y} \frac{\partial Y}{\partial \alpha_i} \delta \alpha_i \right) + Y_- \left(1 - \frac{1}{Y} \frac{\partial Y}{\partial \alpha_i} \delta \alpha_i \right) \right\}^{-1} \\
 &\cong \frac{1}{Y} \frac{\partial Y}{\partial \alpha_i} \delta \alpha_i.
 \end{aligned}$$

This expression is written to first order in $\delta \alpha_i$, the deviation from the helicity average of α_i , where the α_i are parameters such as the beam energy, etc. Finally, since A_{cn} , Y , $\partial Y / \partial \alpha_i$ and $\delta \alpha_i$ are measured in the experiment, the true asymmetry can be calculated

$$A_t = A_m - A_{cn} - \sum_i \frac{1}{Y} \frac{\partial Y}{\partial \alpha_i} \delta \alpha_i.$$

Each of the types of parameter variation are considered below. The required resolutions of the measurement devices for the various parameters are listed in Table 9.

The beam energy enters the yield through the cross section; the derivative of the cross

section with respect to energy is

$$\left| \frac{E_k}{\sigma} \frac{\partial \sigma}{\partial E_k} \right| \cong 4$$

for the forward angle kinematics; the backward angle measurements are less sensitive to changes in the beam energy. Therefore $\delta E_k/E_k$ must be measured to 1×10^{-5} in time T_h .

The beam “diameter” (r.m.s. size) also enters directly – through the effective solid angle. If the beam changes its diameter in a helicity-correlated manner, a false asymmetry will be generated as the solid angle is actually smaller for a larger beam (of the same current). In the case of a uniform beam of diameter d :

$$\left| \frac{d}{\Delta\Omega} \frac{\partial \Delta\Omega}{\partial d} \right| = \frac{1}{4} \left(\frac{d}{r_0} \right)^2$$

where r_0 is the distance from the beam to the solid angle defining aperture. Assuming even a (defocussed) CEBAF beam diameter of $d = 1$ mm and $r_0 \sim 20$ cm (effectively) for the proposed apparatus, $\delta d/d$ must be measured at only about the 100% level. Therefore the effect of the beam size is not significant.

The final parameter which enters the asymmetry directly is the beam intensity. If there is a systematic change in intensity from one helicity to the other, and the intensities are measured with some non-zero helicity-correlated precision, there will be a false asymmetry. However, the relative change in intensity in times on the order of the measurement time is not expected to be large; it was $\sim 1 \times 10^{-2}$ in the Bates ^{12}C experiment [Ku90]. There are actually two contributions from correlated intensity changes: a direct uncertainty in the asymmetry resulting from the uncertainty in the intensity; and a contribution due to the change in detector deadtime in the counting mode. The direct contribution is simply

$$\frac{I}{Y} \frac{\partial Y}{\partial I} \delta I = 1$$

hence $\delta I/I = \delta Q/Q = 4 \times 10^{-5}$ as above (in the absence of non-linearities in the charge measuring device – see Sections 4.4.2 and the Technical Design Report, Section 6.4). The indirect contribution through changes in deadtime is not as important as the direct contribution of deadtime fluctuations to the noise since, for these “induced” changes, there is an extra factor of $\delta I/I$.

The remaining false asymmetries all require a combination of effects, for example, a helicity-correlated beam motion and an (uncorrelated) asymmetry in the spectrometer acceptance. To first order, changes in the beam position and angle are compensated by a perfectly symmetric detector. For the purposes of illustration consider a helicity-correlated beam motion or angle change in the plane of two opposite detectors (“L” and “R”) with

identical acceptances. In the case of beam translation the changes in solid angle are compensated, one side to the other, and in the case of changes in the beam angle, the increased cross section on one side compensates the reduced cross section on the other. However, the opposite segments of the detector will not be perfectly matched. The general form of such effects is

$$A = \left\{ \left[Y_{+R} \left(1 + \frac{1}{Y} \frac{\partial Y}{\partial \alpha} \delta \alpha \right) (1 + \epsilon) + Y_{+L} \left(1 - \frac{1}{Y} \frac{\partial Y}{\partial \alpha} \delta \alpha \right) (1 - \epsilon) \right] - \left[Y_{-R} \left(1 - \frac{1}{Y} \frac{\partial Y}{\partial \alpha} \delta \alpha \right) (1 + \epsilon) + Y_{-L} \left(1 + \frac{1}{Y} \frac{\partial Y}{\partial \alpha} \delta \alpha \right) (1 - \epsilon) \right] \right\} \cdot \{ \text{"sum"} \}^{-1}$$

$$\cong \frac{1}{Y} \frac{\partial Y}{\partial \alpha} \delta \alpha \cdot \epsilon$$

for

$$Y_{+R} = Y_{+L} = Y_{-R} = Y_{-L}$$

where the beam position or angle is represented by α and the efficiency asymmetry for the two detectors is ϵ . For the case of changes in beam position

$$\left| \frac{1}{\Delta \Omega} \frac{\partial \Delta \Omega}{\partial r} \right| = \frac{2}{r_0}$$

where r_0 is again the distance to the solid angle defining aperture. For the case of changes in the angle of the beam with respect to the nominal

$$\left| \frac{1}{\sigma} \frac{\partial \sigma}{\partial \theta'_k} \right| = 570 \frac{1}{\text{rad}}$$

for the forward angle kinematics; again, the backward angle measurement is less sensitive to changes in beam angle. If it is further assumed that the detection asymmetry can be reliably determined at the 5×10^{-3} level (corresponding to the statistics of one 1/30 s measuring period for each detector element), the required precisions for beam position and angle measurements (per 1/30 s measuring period) are

$$\begin{aligned} \delta r &= 800 \mu\text{m} \\ \delta \theta'_k &= 14 \mu\text{r} \end{aligned}$$

The tolerance for the angle measurement corresponds two beam position monitors each with precision of 100 μm at a separation of 10 m.

Changes in beam shape which preserve the first (beam centroid position) and second (the 'diameter' as discussed above) moments of the beam charge distribution also enter the expression for false asymmetries multiplied by a detector efficiency asymmetry. Such

a change could consist of, for example, the third moment simply changing signs. However, such changes result in much smaller asymmetries than those associated with beam diameter changes since they come in like $(d/r_0)^2 \epsilon$ and are certainly smaller than the diameter effects for beams of reasonable shape.

If the beam polarization for positive and negative helicities is different the effect on the physics asymmetry is small. As discussed in Section 4.4.1 the uncertainty in the average polarization enters in the *relative* uncertainty in the physics asymmetry (i.e. if the precision of the polarization measurement is $n\%$, the limiting relative precision of the physics asymmetry will be $n\%$). In contrast, false asymmetries due to helicity-correlated changes in polarization come in only at the level

$$A_f \sim A_{\text{expt}}^2 \frac{\delta P}{P}$$

and are thus unimportant.

4.4.4 Non-linearities

A false asymmetry can result from helicity-correlated changes in beam intensity coupled with a non-linear response in either the spectrometer or the beam charge monitor. As an example, consider the non-linear response of the charge monitor. Suppose that the beam charge Q_0 changes by $\pm\delta Q$ as the helicity changes. If the non-linearity η is defined to be

$$\eta = \left\{ \frac{Q_{\text{meas}}}{Q_0} - \left(1 - \frac{\delta Q}{Q_0} \right) \right\} \cdot \left\{ \frac{\delta Q}{Q_0} \right\}^{-2}$$

for a change of $-\delta Q$ in the beam charge, then

$$A_f \cong \eta \left(\frac{\delta Q}{Q_0} \right)^2.$$

In the absence of measurements of η , this false asymmetry must be less than 5% of the *overall* uncertainty in the experiment, i.e. about 1×10^{-8} . In the Bates ^{12}C experiment the helicity correlated changes in the beam intensity were reduced to be less than 1×10^{-5} averaged over the whole experiment [Ku90], therefore, the relative difference between the measured and true charges must be less than 1×10^{-8} for relative changes in current of 1×10^{-5} or

$$\eta \frac{\delta Q}{Q_0} \leq 10^{-3}.$$

This typical non-linearity tolerance for charge monitor and spectrometer response (measurement interval to measurement interval) should be relatively easy to meet given the

small dynamic range of interest (about 1% from measurement interval to measurement interval).

For the case where detector deadtime (including the case where the deadtime is associated with running pairs of detectors in coincidence) effectively generates a non-linear response, the product $r \cdot \tau$, where r is again the rate and τ is the deadtime, must be less than 10^{-3} . Noting that all three quantities ($\delta Q/Q_0$, r and τ) can in this case be measured, a small correction can be made if needed.

4.4.5 Deadtime

The electronics is such that each detector records at most one pulse during each machine period of 32 ns (see the Technical Design Report, Section 11.2). For back angle electron detection the instantaneous rates are low ($\lesssim 100$ kHz), hence the counting losses are $\lesssim 0.003$. The forward angle proton detection is slightly more complicated. Since we expect roughly equal counting rates of pions and elastic protons and since the pions precede the protons by typically 14 ns, the main effect one needs to consider is the “shadowing” of a legitimate elastic event by a pion. We estimate the effect on the asymmetry of these shadowed events with the following assumptions: equal rates of pions and elastic protons; counting losses of 0.03 (corresponding to 1 MHz rate over 32 ns); equal asymmetries for pion and elastic protons. We find that the measured proton asymmetry is lower than the actual proton asymmetry by 6%. A pion asymmetry twice as large as the proton asymmetry would give rise to a 9% effect, whereas a pion asymmetry of zero would give rise to a 3% effect. In fact, one can correct for this effect if one knows the pion rate and asymmetry, which one can measure by making the appropriate time cut on the data. Therefore the uncertainty in the elastic asymmetry due to deadtime can be reduced to a negligible amount. As discussed in Section 4.4.3, the 2nd order effect due to helicity-correlated differences in beam intensity, giving rise to helicity-correlated differences in the deadtime correction, is also negligible.

4.4.6 Pileup

Since the event rate is expected to be dominated by pions and elastic protons, there are three types of pileup to consider: proton-proton, proton-pion, and pion-pion. With the data rates anticipated in the experiment, the probability for each of these is on the order of a few percent. The principal effect of two particles hitting the same detector is a shift in the apparent time of the event due to the mean-timing technique, as we now discuss.

For the 2-proton or 2-pion events, in which the two particles arrive at different places on the detector at essentially the same time, the net effect is to introduce a small triangular-

shaped tail on the low-time side of the time distribution. The maximum deviation from the nominal time is the product of the half the length of the scintillator (1.4/2 m) and the inverse of the velocity of light in the medium (7.5 ns/m), or about 5 ns. With a time window on the elastic proton events that is tighter than 5 ns, this means that a few percent of good events are lost. As long as the effect is not correlated with helicity (as it could be if the beam current was correlated with helicity and not well measured), it will not affect the measured asymmetry. Our expected $\delta I/I = 4 \times 10^{-5}$ will be sufficient to guarantee this.

For the pion-proton pileup events, we note that the time separation of the pion and proton events (14 ns) is larger than the maximum propagation time of light in the scintillator (10 ns). Therefore the pion-proton pileup events simply get recorded as a pion event with no shift in the apparent time. This becomes part of the deadtime correction, which we already concluded has a negligible effect on the measured asymmetry.

Finally, we intend to instrument some fraction of the detectors to allow us to count coincidences between photomultiplier signals from *different* detectors, thereby allowing us to measure the rate of pileup effects and study their time distribution.

4.4.7 Polarized proton scattering in collimators

Because the recoil protons acquire some polarization from interaction with the polarized electrons in the beam, the analyzing powers of the materials in the target and the collimators from which the protons may scatter can generate scattering asymmetries which may show up as false asymmetries in the parity-violation measurement. This effect is not important for electron detection because the analyzing powers are much smaller (in the absence of polarized scattering materials).

For the first case, the polarized proton scatters from the collimator and is detected at the focal plane. Because the distribution of such scattered protons can have a left-right asymmetry, any misalignment of the detectors can result in a false asymmetry when the beam polarization is flipped (and the proton spin reversed in direction). A GEANT simulation of the combined probability of hitting the detector after scattering from the collimator has been performed with a realistic event generator and median plane magnetic fields. This scattering fraction is $(3.9 \pm 0.9) \times 10^{-4}$ for the lowest momentum protons.

The other factors in the calculation of the false asymmetry are presented in Table 10. The proton polarization is taken to be the maximum of the combined p_x and p_z as spin will rotate in the magnetic field of the spectrometer. The analyzing power is taken at the multiple scattering angle for 1 radiation length of collimator ($\theta_{ms}^{plane} = 8^\circ$ for 320 MeV protons, for example) and the carbon analyzing power is used. The detector asymmetry

Table 10: Terms contributing to the false asymmetry resulting from the scattering of (polarized) 320 and 800 MeV/c protons from collimators in the spectrometer.

	320 MeV/c	800 MeV/c
p_x	0.055	0.23
$A_y(\theta_{ms})$	< 0.1	0.15
detector asymmetry (2 mm @ 1 m)	2×10^{-3}	2×10^{-3}
scattering fraction	4×10^{-4}	< 4×10^{-4}
False Asymmetry	4×10^{-9}	< 3×10^{-8}

is taken to be a worst case alignment tolerance of a 2 mm left-right displacement over its approximately 1 m length. We note that the asymmetry for the $Q^2 = 0.5 \text{ GeV}^2$ point (800 MeV protons) is about five times larger than that for the $Q^2 = 0.1 \text{ GeV}^2$ point; therefore the potentially larger false asymmetry for this case is still well within the conservative limit of 1/20 of the overall systematic uncertainty for any one contribution.

4.4.8 Polarized proton scattering in target

A similar effect can arise from the scattering of the polarized protons through interactions in the liquid hydrogen. In this case, if the target were azimuthally symmetric or if the target were symmetric but displaced and the detectors were azimuthally symmetric, the false asymmetry averaged over all detectors would be zero. Following the same reasoning as in the previous case, the false asymmetries for both extremes of proton energy can be determined as shown in Table 11. Because the hydrogen in the target is a much thinner target for the protons than is a collimator, the scattering angles are much smaller ($\times 1/20$); the analyzing powers are taken to be 5% of those in the case above. Because precise relative counting rate measurements for the detector elements are a byproduct of the asymmetry measurement, they can be used to establish the relative efficiencies for potential false asymmetries of this type. The counting statistics for a single detector corresponding to low (high) proton momentum yield measurements of the relative efficiency with a precision of 5×10^{-4} (7×10^{-3}) in 1/15 s. The target is taken to be offset by 2 mm; this results in a difference in scattering probability for these protons of about 1.2×10^{-4} for the thin and thick parts of the target. We therefore use the (azimuthal) average difference in scattering probability of $1.2/2 \times 10^{-4}$. These false asymmetries are therefore negligible.

Table 11: Terms contributing to the false asymmetry resulting from the scattering of (polarized) 320 and 800 MeV/c protons from a misaligned hydrogen target.

p_x	0.055	0.2
$A_y(\theta_{ms})$	5×10^{-3}	7×10^{-3}
detector asymmetry (1/15 s)	5×10^{-4}	7×10^{-3}
average scattering probability	$\frac{6 \times 10^{-5}}{8 \times 10^{-12}}$	$\frac{6 \times 10^{-5}}{6 \times 10^{-10}}$
False Asymmetry	8×10^{-12}	6×10^{-10}

4.4.9 Particle counting tests

To demonstrate the feasibility of performing a counting experiment to the desired degree of precision, we have started an experimental investigation of the possible problems that might be involved. In earlier parity experiments where counting techniques have been used, uncertainties of about 6×10^{-6} have been achieved without any particular problems associated with the measurement technique [Ze89]. Before reaching a final decision regarding counting, we would like to have demonstrated that a high precision counting experiment is feasible by measuring an asymmetry with a precision of about 1×10^{-7} with the electronics to be used in the experiment.

The experimental set up used in the initial tests is shown in Figure 15. Two radioactive sources viewed by plastic scintillators connected to photomultiplier tubes are used to provide random pulses. One of the sources is a high intensity source and is used as the main signal, while the other, much weaker source, produces a controlled asymmetry when added to the main signal. A random pulser has been used in place of the weak source for the most recent runs. The phototubes are connected to gated discriminators. The main signal is fanned out to two scalars; the weaker signal is added (via a linear fan-in) to the input of one of the scalars during alternate gates.

By separately counting the number of pulses added to the main signal, the actual asymmetry can be determined. If the summed signal measurement is done properly, the calculated asymmetry from this measurement should agree with the actual asymmetry within statistics. Results from initial test show that this is indeed the case, at least at the precision achieved so far. Two tests have been done. In the first the low rate source was

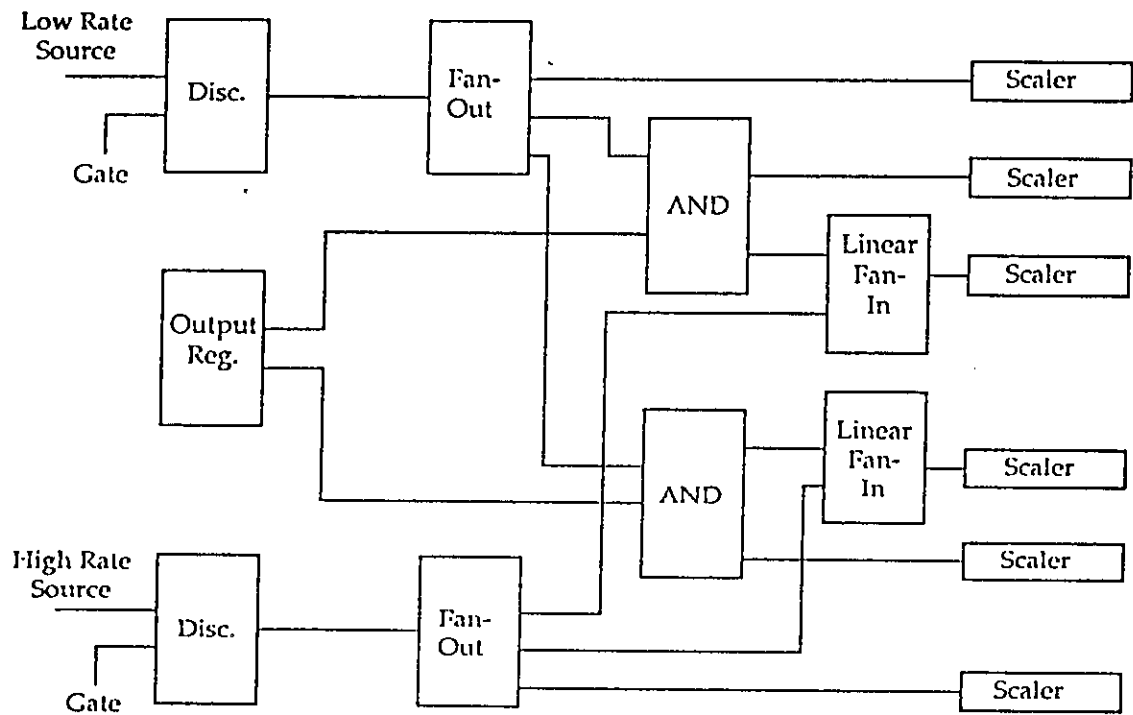


Figure 15: Electronic setup used for the counting tests.

“turned off” in order to try to simply measure zero. The result is:

$$\begin{aligned} A &= (-0.1 \pm 3.0) \times 10^{-7} && \text{(Measured)} \\ A &= 0.0 && \text{(Actual).} \end{aligned}$$

The average rate in each of the 10 scintillator elements was 1.8 MHz for this test. In the second test the low rate was set to produce an asymmetry comparable to those to be measured in the experiment. The result is

$$\begin{aligned} A &= (67.4 \pm 2.8) \times 10^{-7} && \text{(Measured)} \\ A &= 65.6 \times 10^{-7} && \text{(Actual)} \end{aligned}$$

The errors shown are due to statistics only. A small correction was made for deadtime in the latter case (reducing the asymmetry from 66.9×10^{-7}); the average rates (four elements) were 1.3 MHz. Scalers with a speed of 200 MHz were used throughout. The measurement intervals for the latter case were only approximately 1/60 s with no apparent consequence; furthermore, the “helicity pattern” $- + + -$ was used throughout (in lieu of choosing this pattern or its complement randomly). Therefore, there are in principle at least two aspects of the tests where we could be more careful if needed. In summary, at this level of accuracy there are no obvious difficulties encountered in measuring asymmetries by counting individual particles.

4.5 Analyzing asymmetry data in the presence of background

As discussed in previous sections of this document, we expect backgrounds from pions, neutrons, and inelastic protons (for the forward angle measurements). Crucial to our ability to separate these backgrounds from the desired events (elastic protons) is the time-of-flight technique. For each 1ns time bin, we measure an asymmetry A . This asymmetry is related to the elastic asymmetry A_e (due to elastic protons) by the following expression:

$$A = \frac{A_e R_e - A_b R_b}{R_e + R_b},$$

where R_e and R_b are the total counting rates for the elastic and background events, respectively, and A_b is the asymmetry of the background events. All of these quantities may be functions of time. Although we have some knowledge of how large R_b can be (see Section 3.3), we have no knowledge of A_b . Our plan is to, in effect, *measure* A_b by finding a time bin where the background dominates. By measuring both the helicity-averaged event rates and the asymmetries as a function of time, it should be possible to correct for the background.

We now ask how different A can be from A_e based on what we now know. First we note that for a given time bin, if there is no background ($R_b = 0$) or if the background and elastic asymmetries are equal ($A_e = A_b$), then $A = A_e$. On the other hand, suppose there is a background of roughly 5% in the time bin corresponding to most of the elastic events. Then if $A_b = (0 - 2) \times A_e$, $A = (1.00 \pm 0.05)A_e$. If these estimates are reasonable, then the measured asymmetry deviates from the elastic asymmetry by $\approx \pm 5\%$. If our technique of *correcting* for the background is successful, we should be able to reduce the uncertainty in A_e due to background to $\approx \pm 2\%$.

5 Budget

5.1 Overall budget

The budget for the G0 experiment is presented in Tables 12 – 14. The numbers in the present section are the best estimates of the engineering group associated with the project. They are based primarily on the independent cost estimate of Powers Associates. In all cases the estimates of the G0 engineering group are equivalent to or slightly higher than those in the independent estimate (see Section 5.2). **Note that all costs are quoted in constant 1993 \$.**

Engineering, design, inspection and acceptance (EDIA) costs are included in the estimate for the spectrometer at rates of 10 - 20% depending on the type of activity. Contingency is included in the spectrometer estimate at a rate of 25% of equipment plus EDIA. Costs for the smaller subsystems are the usual equipment costs quoted in, for example, on-going grant proposals.

The total cost of the experiment is outlined in Tables 13 – 14. The estimated total cost is \$4.097M. Of this, \$2.298M would be new money requested from the NSF and \$0.283M would be new money requested from the DOE. The remainder, \$1.516M would be contributed from continuing grants including \$1.136M from CEBAF operations. A possible profile for the new NSF money is shown in Figure 16.4. The new money requested from NSF may be reduced by in-kind contributions from the China Institute of Atomic Energy.

5.2 Comparison of Powers Associates and Elin cost estimates

In Table 15 we present the comparison of the cost estimates for spectrometer components from Powers Associates and Elin Energieanwendung. Elin estimated prices for superconducting and mechanical components. This job is comparable to the HMS superconducting coil/cryostat recently completed by Elin for CEBAF.

As one would expect, because of the particular manufacturing capabilities of a specific vendor, in detail the prices of the components are not equivalent. In addition, assembly labor is folded in to the Elin estimate item by item to a greater extent. We note that the differences in cost for individual components are $\leq 13\%$ of the total (excluding the labor item 'Assembly Labor and Tooling'), and that the totals comparable.

Table 12: G0 budget detail

Item	Equip (k\$)	EDIA (k\$)	Cont. (k\$)	Total (k\$)	Total (k\$)	Resp. Inst.
<i>Spectrometer</i>						
Superconductor	300	30	83	413		CEBAF
Coil & Case	390	78	117	585		UIUC/CIAE
Coil Support	80	16	24	120		UIUC/CIAE
Collimators, Line-of-sight Shielding	137	27	41	206		UIUC/CIAE
LHe Plumbing	179	36	54	268		UIUC/CIAE
LN2 Shield	24	5	7	36		UIUC/CIAE
Cryostat	210	42	63	315		UIUC/CIAE
Carriage	25	5	8	38		UIUC/CIAE
Detector Support	25	5	8	38		UIUC/CIAE
Scintillator Shielding	15	3	5	23		UIUC/CIAE
Assembly Labor & Tooling	300	45	86	431		UIUC/CIAE
Vacuum System	60	6	17	83		CEBAF
Power Supply	60	6	17	83		CEBAF
Control Systems	80	16	24	120		UIUC/CIAE
Shipping	30	3	8	41		UIUC/CIAE
CEBAF Assembly						
Labor & Tooling	70	7	19	96		CEBAF
Hall Cabling	40	4	11	55		CEBAF
External Shielding	75	15	23	113		CEBAF
Subtotal	2100	349	612	3061	3061	UIUC/CIAE + CEBAF
<i>Detectors</i>						
Scintillator	25					RPI
Lightguides	20					RPI
Phototubes	75					RPI
Bases, Shields	48					RPI
Gain Monitoring	30					RPI
Assembly	11					RPI
Subtotal	209				209	RPI
<i>Electronics</i>						
Clock Distribution	13					CMU
Mean-timers	29					CMU
CFD's	57					CMU
Shift Register Boards	28					CMU
Scalers	140					CMU
Fastbus ADC's, TDC's	39					CMU
Splitters, etc.	17					CMU
Bins, Cables, Crates	95					CEBAF
H.V. Power Supply	42					CEBAF
DAQ Computer Station	35					CEBAF
DAQ Electronics Modules	18					CEBAF
Subtotal	512				512	CMU+CEBAF
<i>Target</i>						
Gas Panel	50					Caltech/UMd
Target Cell	60					Caltech/UMd
Moving Mechanism	35					Caltech/UMd
Plumbing	65					Caltech/UMd
Subtotal	210				210	Caltech/UMd
<i>Beamline</i>						
Electron Polarimeter Modifications	30					CEBAF
Beam Current, Position Monitors	75					CEBAF
Subtotal	105				105	CEBAF
Grand Total					4097	

Table 13: G0 Budget Summary

Item	Equip (k\$)	EDIA (k\$)	Cont. (k\$)	Total (k\$)
Spectrometer	2100	349	612	3061
Dectectors	209			209
Electronics	512			512
Target	210			210
Beamline	105			105
Total	3136	349	612	4097

Table 14: G0 Budget Contributions

Item	Home Inst'n (k\$)	CEBAF Ops (k\$)	NSF (new) (k\$)	DOE (new) (k\$)	Total (k\$)
Spectrometer	300	841	1920		3061
Detectors	11		198		209
Electronics	39	190		283	512
Target	30		180		210
Beamline		105			105
Total	380	1136	2298	283	4097

Table 15: Comparison of estimates for spectrometer components from Powers Associates and Elin Energieanwendung. Powers Associates estimates include 15% EDIA and 25% contingency.

Item	Internal (k\$)	Powers (k\$)	Elin (k\$)	Elin - Powers (k\$)
<i>Spectrometer</i>				
Superconductor plus Coil & Case	998	992	720	-272
Coil Support	120	89	154	+65
Collimators, Line-of-sight Shielding	206	151	170	+19
LHe Plumbing	268	250	384	+134
LN2 Shield	36	35	45	+10
Cryostat	315	277	557	+280
Carriage	38	36	127	+91
Assembly Labor & Tooling	431	431	63	-368
Total	2412	2261	2220	-41

6 Schedule

A preliminary project schedule has been created for the G0 equipment fabrication. The near term goal is to complete enough of the engineering to allow for coil construction beginning in October 1994. The spectrometer fabrication and assembly is expected to take about two years (consistent both with the Elin estimate and the time required for the HMS dipole fabrication). Spectrometer construction is the overall critical path item; target, detectors and electronics are required as the testing phase is approached. Overall assembly and testing of the entire apparatus is expected to take place at the University of Illinois. It would then be disassembled in the largest possible pieces and shipped to CEBAF.

The preliminary 'network' (PERT) chart outline for the project is shown in Figure 16. The accompanying timeline (Gantt) chart is shown in Figure 17. As is shown, we expect that equipment fabrication, assembly and testing will be completed late in calendar 1996 with installation at CEBAF to follow. The specific critical path item identified here is the construction of the cryogenic system (reservoir, etc.) which is not scheduled to begin until the start of FY1996 in order to level the new money requests from NSF. The earliest anticipated arrival among the target, detector and electronics subsystems is for the detectors - 3Q FY96.

As mentioned above, the overall critical path item is the spectrometer, and the near term need is to complete the engineering required for the reference conceptual design (RCD). The anticipated distribution of engineering resources for the complete spectrometer project is shown in Figure 18. These data are also listed in Table 16.

In the first year, the coil fabrication dominates; the expected duration is about 1 year (consistent with the HMS coil construction time). Other necessary components are constructed to allow the coils to be placed first on the assembly fixture and then suspended within the cryostat early in FY1996.

The second year fabrication is largely confined to the cryogenic system and cryostat heads. We expect to have the cryogenic system installed by approximately the beginning of 3Q FY1996. Testing would begin in the summer of 1996 and be completed by the end of the year.

The largest sum of new money would be requested from the NSF. *For the spectrometer fabrication alone* (as shown in Figure 19, and listed in Table 16), the initial requirement is for \$171k (constant 1993 \$ in all cases) to complete the RCD in time to begin coil construction at the start of FY1995. Thereafter, the requests are approximately equal: \$870k and \$879k in FY1995 and FY1996; all contingency is delayed until FY1996 in this

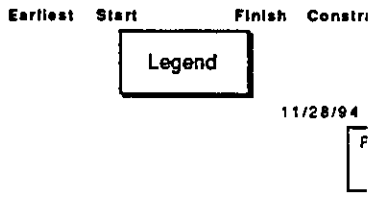
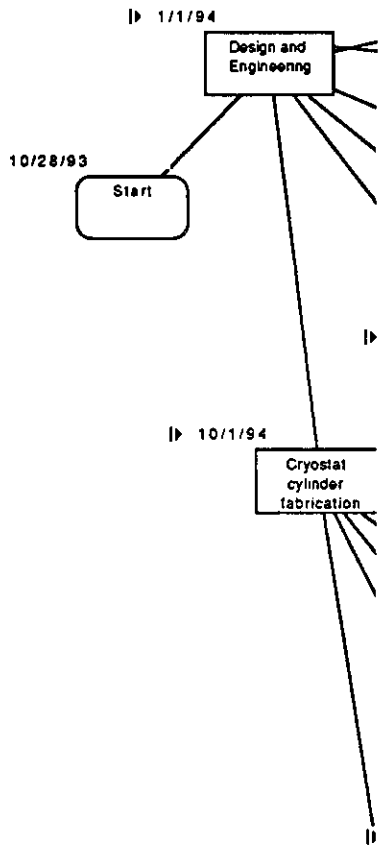


Figure 16.1: Preliminary

Name	107
Start	
Design and Engineering	
Prototyping and tests	
Shielding module fab.	
Coil support fab.	
Coil fab. and winding	
Cryostat cylinder fabrication	
Carriage fab.	
Assembly tooling fab.	
Target arrives	
Electronics arrive	
Schibitor and L.G. Arrives	
Carriage Assy	
LN2 Radiation Shield Fab.	
Poly shielding fabrication	
Detector support fab.	
LN2 shield installed in cryostat	
Coil sub-assy on fixture	
Cold/Warm support fab.	
Cryogenic reservoir fab.	
Control fab. and test	
Power supply procurement	
Vacuum system procurement	
Rotating Lifting fixture fab.	
Head fabrication	
PMTs arrive	
Shielding module assy into fixture	
Cold mass insertion in cryostat	
Cryogenic plumbing installed	
Detector/shield module assy	
Detector/shield modules installed on DS head	
Cryostat mounted on carriage	
PMTs install-d	
Detector testing	
Cryo system testing at UIUC	
Final testing	
Shipping to CEBAF	
Installation in Hall C	

Figure 16.2: Prelimir

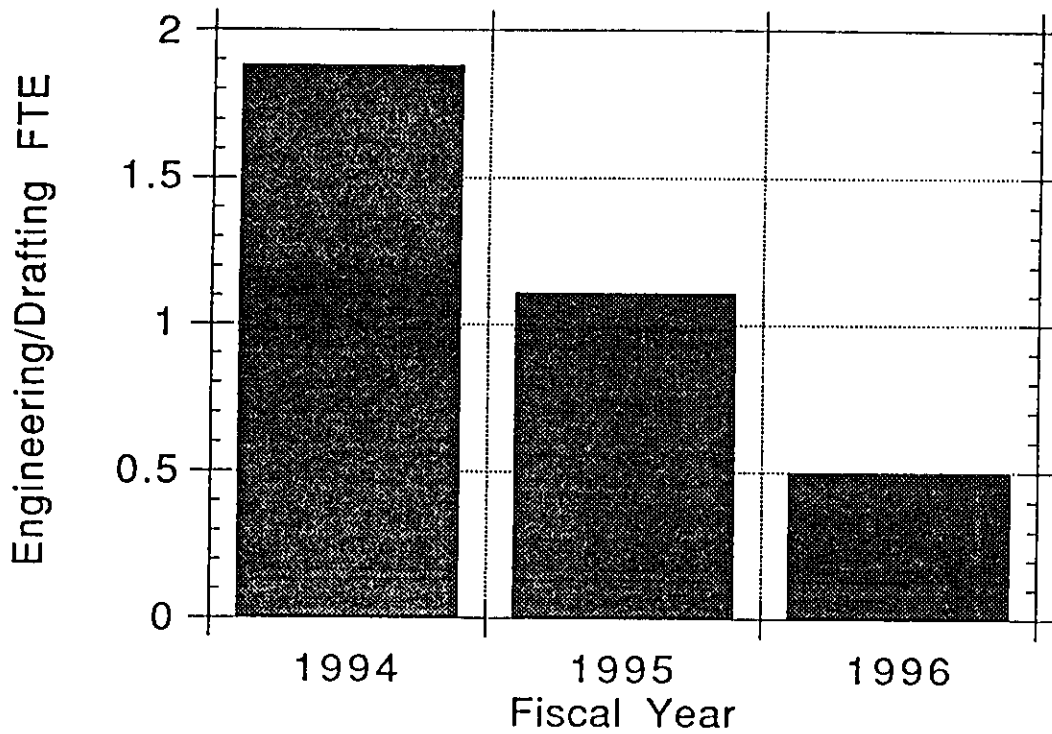


Figure 18: Preliminary distribution of engineering resources for the G0 spectrometer fabrication project.

breakdown. These costs may be reduced by in-kind contributions from CIAE. Assuming an equal division of funds in FY 1995 and FY1996 for the target and detectors, the total requests would be \$1059k in FY 1995 and \$1068k in FY1996.

Table 16: Preliminary distribution of resources for the spectrometer fabrication project.

Fiscal Year	Engineering FTE (yr)	Engineering Expenditure (k\$)	New NSF Spectrometer (k\$)	New NSF Total (k\$)
1994	1.88	171	171	171
1995	1.11	127	870	1059
1996	0.50	53	879	1068
Total	3.49	351	1920	2298

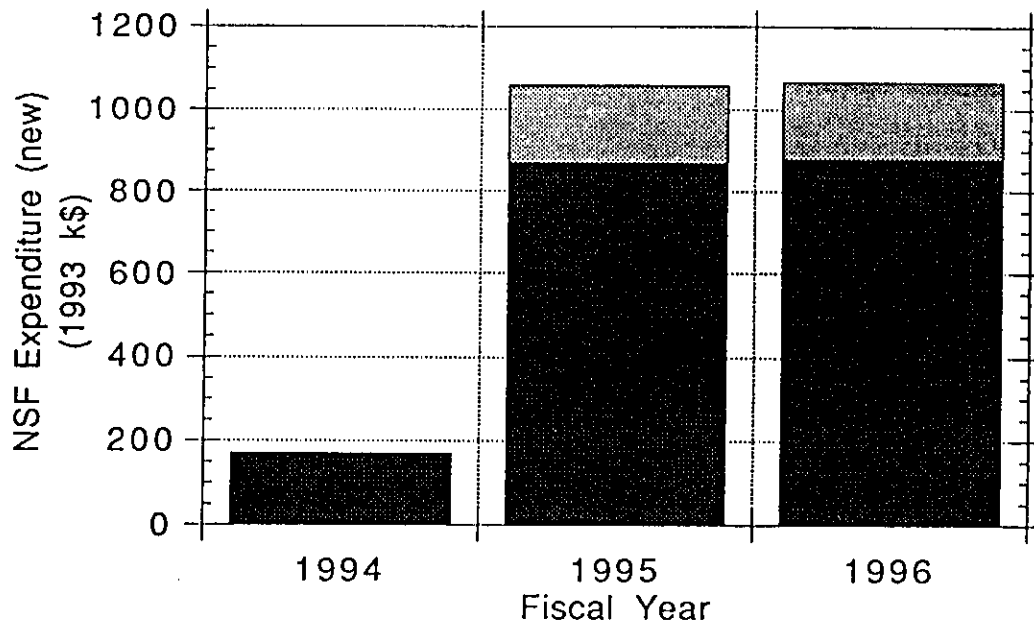


Figure 19: Profile of new money requests from the NSF (spectrometer – dark, target and detectors – light).

7 Beam time request

We request a total of 3940 h of beam time to complete measurements of forward and backward asymmetries in the range $0.1 \leq Q^2 \leq 0.5 \text{ GeV}^2$ as outlined in Section 3. This time is divided among commissioning (1100 h), forward asymmetries (700 h) and backward asymmetries (2140 h). As is shown in Table 17, all the forward angle measurements are made simultaneously; backward angle measurements are made for each of the four momentum transfers.

Table 17: Beam time request.

	Energy (GeV)	Q^2 (GeV ²)	Time (h)
Commissioning	3.0		1100
Forward asymmetries	3.0	0.1 – 0.5	700
Backward asymmetries	0.2	335	390
	0.3	428	470
	0.4	512	580
	0.5	590	700

A preliminary commissioning plan has been formulated. We anticipate breaking this time into three runs of approximately 2 weeks each (running with the fully instrumented spectrometer and the liquid hydrogen target). The details of the measurements for the three runs are as follows:

1. Run 1

- check spectrometer optics (shape of constant Q^2 locus at focal surface, etc.): 3 days
- backgrounds: external shielding, set field to low value to investigate neutrons and γ 's: 4 d
- detector efficiencies, ADC and TDC spectra, overall device symmetry: 2 d
- first asymmetries: 3 d
- empty target (background, symmetry, etc.): 2 d

2. Run 2

- more background studies: 4 d
- begin to establish procedure for centering beam with respect to target and detector: 2 d
- begin measurement of correlated parameter derivatives (yield with respect to beam position, etc.): 2 d
- asymmetry test (correct with measured coefficients): 5 d
- studies of beam polarization (current dependence of polarization): 1 d

3. Run 3

- final procedure for centering: 3d
- final correlated parameter derivative study: 4 d
- asymmetry test: 7 d

8 Appendix A

Barish Committee questions

- Q1. What false asymmetry results from the analyzing power of elastic protons scattering from a) collimator edges, b) LH₂ in the target?
- A1. a) The false asymmetry for scattering of polarized protons from the collimator edges is estimated to be $< 3 \times 10^{-8}$ (recall that the goal for false asymmetries was $A_{false} \leq 2.5 \times 10^{-7}$). The scattering probability for this situation has been determined in a GEANT simulation. We continue to explore options both for reducing these false asymmetries and for measuring such asymmetries during data-taking.
- b) The false asymmetry for scattering of polarized protons from the target LH₂ requires the target to be azimuthally asymmetric (eg. target misaligned). For a misalignment of 2 mm, the false asymmetry is estimated to be 6×10^{-10} .
- Q2. Are the back angle measurements optimized?
- A2. Adjustable collimators are used in the spectrometer allow the largest angular acceptance consistent with resolution of elastic electrons. It is not possible to increase significantly the backward angle acceptance without a severe compromise in the forward angle measurements and/or a very significant increase in cost.
- Q3. Can the back angle measurements be extended?
- A3. The back angle measurements can be extended (using the adjustable collimators to define the acceptance) such that measurements with $\Delta A_{stat}/A = 0.10$ can be made for $Q^2 \leq 3 \text{ GeV}^2$ in about one month of beam time per measurement (Section 2.4). It might also be possible to extend the forward angle measurements to $Q^2 = 1 \text{ GeV}^2$ with comparable statistical precision in a separate measurement of one month duration.
- Q4. Is the design of the spectrometer optimized?
- A4. The superconducting option has been chosen to minimize the combined fabrication and operating costs. Both the resistive and superconducting versions have been optimized in terms of coil number and size subject to the constraints of the physics program and of hall access and maximum overall size. The layout and design of the spectrometer, including the superconducting coil geometry, has simplified as much as possible.

Q5. Should a superconducting design be considered? Does the spectrometer have other uses?

A5. The superconducting option has been adopted (see A4.). It may be possible to use such a spectrometer to measure angular distributions ("out-of-plane") of final state hadrons, for example, with the spectrometer axis set along the momentum transfer direction. An example of such a use is in the analysis of partial wave amplitudes contributing to nucleon resonance production. Other uses are being contemplated by other groups. The primary emphasis is on the spectrometer's use in a program of parity-violating electron scattering measurements.

Q6. Can the time-of-flight timing be improved from 2 to 1 ns?

A6. The timing has been improved by adding a second parallel shift register and four new scaler channels per detector element. The cost increment is estimated to be \$50k.

PAC questions

Q1. Is a superconducting option cost-effective?

A1. Yes, see A4. above.

Q2. Is the detector system for electrons adequate? Should Čerenkov counters be part of the detector package?

A2. Based on measurements at UIUC-NPL, single scintillator detectors appear to be adequate for electron detection in the range $0.2 \leq Q^2 \leq 0.5 \text{ GeV}^2$; π^- are kinematically forbidden for the incident energies used in these cases. For higher momentum transfer measurements and for measurements in deuterium, Čerenkov detector elements may be required. These are considered to be a second stage addition to the basic system and would be funded separately.

Q3. Can the polarized source be operated effectively in the chopped, increased peak current mode?

A3. The chopping can be effected using a mode-locked laser. The required peak current is available from bulk or thin GaAs crystals; it may also be possible to obtain it reliably from strained crystals. The optimum frequency for the laser is 31.25 MHz. In the worst case present experiments indicate that high polarization crystals have sufficient quantum efficiency to operate with a 93.75 MHz laser, and generate approximately 40 μA for the experiment after eliminating 2/3 pulses with a supplementary r.f. chopper.

Q4. Can the beam polarization be reliably measured to 3%?

A4. A beam polarimeter with performance expected at the 1% level is being constructed for Hall C (for low average beam currents). The chopped beam for the G0 experiment can be reduced in duty cycle to meet this average beam current limitation. Therefore, even if the polarimeter does not meet its design goals it seems likely that 3% is within reach.

Q5. What is the total cost of the experiment?

A5. See summary in Section 1; see also the 'Budget' section.

References

- [Ab82] H. Abramowicz *et al.* (CDHS) *Z. Phys.* **C15** (1982) 19.
- [Ad93] B. Adeva, *et al.* (SMC Collaboration) *Phys. Lett.* **B362** (1993) 553.
- [Ah87] L. Ahrens, *et al.* *Phys. Rev.* **D35** (1987) 785.
- [An93] P. Anthony, *et al.* (E142 Collaboration) *Phys. Rev. Lett.* **71** (1993) 959.
- [As89] J. Ashman *et al.*, *Nucl. Phys.* **B328** (1989)1.
- [Ba81] N. Baker, *et al.*, *Phys. Rev. D* **23** (1981) 2499.
- [Be89] D. Beck, *Phys. Rev. D* **39** (1989) 3248.
- [Be91] CEBAF experiment 91-004, E. Beise spokesperson.
- [Be92] D. Beck, in *Symmetry and Spin in the Standard Model*, ed. B. Campbell, L. Greeniaus, A. Kamal, and F. Khanna (World Scientific, Singapore, 1992), and references therein.
- [Ca78] R. N. Cahn and F. J. Gilman, *Phys. Rev. D* **17** (1978) 1313.
- [Co93] T. Cohen, H. Forkel and M Nielsen, University of Maryland preprint 93-217 (1993).
- [De68] H. DeStaebler and T. M. Jenkins, in *The Stanford 2 Mile Accelerator*, R. B. Neal, ed. (Benjamin, New York, 1968) pp. 1035ff, especially Figure 26-8.
- [Do89] J. Donoghue, *Ann. Rev. Nucl. Part. Sci.* **39** (1989) 1.
- [Fi91] CEBAF experiment 91-010, M. Finn and P. Souder spokespersons.
- [Ga93] G. Garvey, W. Louis and H. White, *Phys. Rev. C* **48** (1993) 761, and priv. comm.
- [Ha92] E. Hadjimichael, G. I. Poulis and T. W. Donnelly, MIT preprint CTP#2041.
- [Ho76] G. Höhler, *Nucl. Phys.* **B114** (1976) 505.
- [Ho93] S. Hong and B. Park, *Nucl. Phys.* **A561** (1993) 525.
- [Ja89] R. L. Jaffe, *Phys. Lett.* **229B** (1989) 275.
- [Ka88] D. Kaplan and A. Manohar, *Nucl. Phys.* **B310** (1988) 527.

- [Ki83] T. Kitagaki, et al., Phys. Rev. D **28** (1983) 436.
- [Ku90] K. Kumar, Syracuse University Ph.D. thesis (1990), unpublished.
- [LA81] *MCNP- A General Monte Carlo Code for Neutron and Photon Transport LA-7396-M Revised*, Los Alamos National Laboratory (April, 1981)
- [Li88] J. Lightbody and J. O'Connell, Computers in Physics **2** (1988) 57.
- [Ma84b] W. J. Marciano and A. Sirlin, Phys. Rev. D **29** (1984) 75.
- [Ma84a] A. Manohar and H. Georgi, Nucl. Phys. **B234** (1984) 189.
- [Ma84b] W. J. Marciano and A. Sirlin, Phys. Rev. D **29** (1984) 75.
- [Mc89] R. D. McKeown, Phys. Lett. **219B** (1989) 140.
- [Mi82] K. Miller, et al., Phys. Rev. D **26** (1982) 537.
- [Mu90] M. J. Musolf and B. R. Holstein, Phys. Lett. **242B** (1990) 461.
- [Mu93a] M. Musolf and M. Burkardt, CEBAF preprint TH-93-01 (1993).
- [Mu93b] M. Musolf, et al. CEBAF preprint # TH-93-11, submitted to Ann. Phys.
- [Na91] J. Napolitano, Phys.Rev. C **43** (1991) 1473.
- [Pa91] N. Park, J. Schechter and H. Weigel, Phys. Rev. D **43** (1991) 869.
- [Pr89] R.E. Prael, H. Lichtenstein, Group X-6, *User Guide to LCS: The LAHET Code System* Los Alamos National Lab, Revised Sept 15, 1989
- [We90] S. Weinberg, Phys. Rev. Lett. **65** (1990) 1181.
- [Ze89] V. Zeps, Ph.D. thesis, University of Washington, 1990 (unpublished).